

**UCLA**  
**COMPUTATIONAL AND APPLIED MATHEMATICS**

---

**Wavelet-Based Numerical Homogenization  
with Applications**

**Bjorn Engquist  
Olof Runborg**

**April 2001  
CAM Report 01-14**

---

**Department of Mathematics  
University of California, Los Angeles  
Los Angeles, CA. 90095-1555**

**<http://www.math.ucla.edu/applied/cam/index.html>**

# Wavelet-Based Numerical Homogenization with Applications

Björn Engquist<sup>1</sup> and Olof Runborg<sup>2</sup>

<sup>1</sup> University of California, Los Angeles, Department of Mathematics, Los Angeles, CA, 90095-1555 and Royal Institute of Technology, Department of Numerical Analysis and Computer Science, 100 44, Stockholm

<sup>2</sup> Princeton University, PACM, Department of Mathematics, Princeton, NJ, 08544-1000

**Abstract.** Classical homogenization is an analytic technique for approximating multiscale differential equations. The numbers of scales are reduced and the resulting equations are easier to analyze or numerically approximate. The class of problems that classical homogenization applies to is quite restricted. We shall describe a numerical procedure for homogenization, which starts from a discretization of the multiscale differential equation. In this procedure the discrete operator is represented in a wavelet space and projected onto a coarser subspace. The wavelet homogenization applies to a wider class of problems than classical homogenization. The projection procedure is general and we give a presentation of a framework in Hilbert space, which also applies to the differential equation directly. The wavelet based homogenization technique is applied to discretizations of the Helmholtz equation. In one problem from electromagnetic compatibility a subgrid scale geometrical detail is represented on a coarser grid. In another a wave-guide filter is efficiently approximated in a lower dimension. The technique is also applied to the derivation of effective equations for a nonlinear problem and to the derivation of coarse grid operators in multigrid. These multigrid methods work very well for equations with highly oscillatory or discontinuous coefficients.

## 1 Introduction

In the numerical simulation of partial differential equations, the existence of subgrid scale phenomena poses considerable difficulties. With subgrid scale phenomena, we mean those processes which could influence the solution on the computational grid but which have length scales shorter than the grid size. Fine scales in the initial values may, for example, interact with fine scales in the material properties and produce coarse scale contributions to the solution.

There are traditional ways to deal with this problem. A number of methods exist, which are based on physical considerations for a specific application, such as turbulence models in computational fluid dynamics, [44], and analytically derived local subcell models in computational electromagnetics, [42]. Geometrical optics or geometrical theory of diffraction approximations of high frequency wave propagation are other classical techniques to overcome the difficulty of highly oscillatory solutions, [28].

All these techniques result in new sets of approximative equations that do not contain the small scales, but which anyway attempt to take the effect of these scales

into account. A more general analytical technique for achieving this goal is classical homogenization, which will be discussed below.

If the small scales are localized, there are some numerical procedures which are applicable. Local mesh refinement is quite common but could be costly if the small scales are very small or distributed. There are also problems with artificial reflections in mesh size discontinuities and time step limitations for explicit techniques. Numerical shock tracking or shock fitting can also be seen as subgrid models, [1]. Material interfaces can be handled by grid adaptation or the immersed interface method, [32].

In this paper we present a general procedure for constructing subgrid models to be used on a coarse grid where the smallest scales are not resolved. The objective is to find models that accurately reproduce the effect of subgrid scales and that in some sense are similar to the original differential operator. The starting point is a finite-dimensional approximation of a differential equation. Let  $L_\varepsilon$  be a linear differential operator for which  $\varepsilon$  indicates small scales in the coefficients. The solution  $u_\varepsilon$  of the differential equation

$$L_\varepsilon u_\varepsilon = f_\varepsilon, \quad (1)$$

will typically inherit the small scales from the operator  $L_\varepsilon$  or the data  $f_\varepsilon$ . Consider for example the simple model problem

$$L_\varepsilon u_\varepsilon = -\frac{d}{dx} \left( g^\varepsilon(x) \frac{d}{dx} \right) u_\varepsilon(x) = f(x), \quad 0 < x < 1, \quad (2)$$

$$u_\varepsilon(0) = u_\varepsilon(1) = 0. \quad (3)$$

The coefficient  $g^\varepsilon(x)$  may be oscillatory,

$$g^\varepsilon(x) = g(x/\varepsilon), \quad g(y) \text{ 1-periodic}, \quad (4)$$

or have a localized sharp transition,

$$g^\varepsilon(x) = \begin{cases} g_1, & x < (1 - \varepsilon)/2, \\ g_2, & (1 - \varepsilon)/2 \leq x < (1 + \varepsilon)/2, \\ g_1, & x \geq (1 + \varepsilon)/2. \end{cases} \quad (5)$$

Our goal is to find an accurate and computationally efficient finite dimensional approximation of (1),

$$\bar{L}_{\varepsilon\Delta} \bar{u}_{\varepsilon\Delta} = \bar{f}_{\varepsilon\Delta}. \quad (6)$$

Difficulties originate from the small scales or high frequencies in (1). If  $\varepsilon$  denotes a typical wave length in  $u_\varepsilon$  and  $h$  a typical element size or step size in (6), then  $h$  must be substantially smaller than  $\varepsilon$  in order to resolve the  $\varepsilon$ -scale in the numerical approximation. This can be costly if  $\varepsilon$  is small compared to the overall size of the computational domain. Ideally the discretized operator in (6) should be designed such that  $\bar{u}_{\varepsilon\Delta}$  is a good approximation of  $u_\varepsilon$  even if  $h$  is not small compared to  $\varepsilon$ . This goal resembles that of classical analytical homogenization.

## 1.1 Classical Homogenization

Homogenization is a well established analytical technique to approximate the effect of smaller scales onto larger scales in multiscale differential equations. There are

explicit formulas for some classes of problems with periodic or stochastic coefficients. The problem is often formulated as follows. Consider a set of operators  $L_\varepsilon$  in (1), indexed by the small parameter  $\varepsilon$ . Find the limit solution  $\bar{u}$  and the *homogenized operator*  $\bar{L}$  defined by

$$L_\varepsilon u_\varepsilon = f, \quad \lim_{\varepsilon \rightarrow 0} u_\varepsilon = \bar{u}, \quad \bar{L}\bar{u} = f. \quad (7)$$

In certain cases the convergence above and existence of the homogenized operator can be proved, [5].

For simple model problems, with coefficients that are periodic on the fine scale, exact closed form solutions can be obtained. For instance, with  $g(y)$  positive, 1-periodic and bounded away from zero, we have for the one-dimensional example (2),

$$L_\varepsilon = -\frac{d}{dx} \left( g(x/\varepsilon) \frac{d}{dx} \right), \quad \bar{L} = -\hat{g} \frac{d^2}{dx^2}, \quad \hat{g} = \left( \int_0^1 \frac{dy}{g(y)} \right)^{-1}. \quad (8)$$

With the same  $\hat{g}$  we get for the hyperbolic operators,

$$L_\varepsilon = \frac{\partial}{\partial t} + g(x/\varepsilon) \frac{\partial}{\partial x}, \quad \bar{L} = \frac{\partial}{\partial t} + \hat{g} \frac{\partial}{\partial x}. \quad (9)$$

These model examples are used in Sect. 4.1 and Sect. 4.2.

In higher dimensions, the solution to (7) is a little more complicated, although for some model problems the structure of the homogenized operator can still be written down, as long as the coefficients are periodic or stochastic. In the  $d$ -dimensional elliptic case, let  $G(y) : \mathbb{R}^d \mapsto \mathbb{R}^{d \times d}$  be uniformly elliptic and  $q$ -periodic in each of its arguments. Let  $I_d$  denote the unit square. It can then be shown, [5], that

$$L_\varepsilon = -\nabla \cdot \left( G \left( \frac{x}{\varepsilon} \right) \nabla \right), \quad \bar{L} = -\nabla \cdot (\hat{G} \nabla), \quad \hat{G} = \int_{I_d} G(y) - G(y) \frac{d\chi(y)}{dy} dy, \quad (10)$$

where  $d\chi/dy$  is the jacobian of the function  $\chi(y) : \mathbb{R}^d \mapsto \mathbb{R}^d$ , given by solving the so called cell problem,

$$\nabla \cdot G(y) \frac{d\chi(y)}{dy} = \nabla \cdot G(y), \quad y \in I_d, \quad (11)$$

with periodic boundary conditions for  $\chi$ . Note that  $\hat{G}$  is a constant matrix.

## 1.2 Numerical Homogenization

Classical homogenization is very useful when it is applicable. The original problem with small scales is reduced to a homogenized problem that is much easier to approximate numerically. See the left path in Fig. 1. The subscript  $\Delta$  indicates numerical approximation. If analytical homogenization is not possible, numerical homogenization should be applied in order to arrive at a method with reasonable computational complexity. With numerical homogenization, we mean a technique to produce a discrete operator  $\bar{L}_{\varepsilon\Delta}$  such that  $\|u_\varepsilon - \bar{u}_{\varepsilon\Delta}\|$  is small and where the complexity of solving  $\bar{L}_{\varepsilon\Delta} \bar{u}_{\varepsilon\Delta} = \bar{f}_{\varepsilon\Delta}$  does not grow fast with  $\varepsilon^{-1}$ .

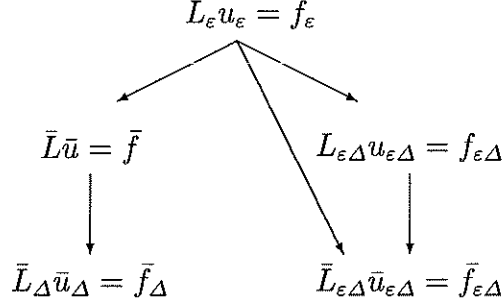


Fig. 1. Schematic steps in homogenization

The numerical homogenization can be done directly as indicated by the middle path in Fig. 1, or by first discretizing the original problem and then compressing the operator  $L_{\epsilon\Delta}$  and the data  $f_{\epsilon\Delta}$  as indicated by the right path. In this paper we shall present wavelet based methods in order to achieve numerical homogenization. We will consider the case of compressing a discretized problem but the technique could also be used for direct discretization.

There are other similar methods based on coarsening techniques from algebraic multigrid, see for example, Knapek [29] and Neuss et. al. [35,34]. In the finite element setting there are a few successful methods for numerical homogenization. In the work of Hughes and collaborators [26,25], Hou and collaborators [16,24] and also in Matache and Schwab [33], the effect of the microstructure is incorporated in a Galerkin framework.

### 1.3 Wavelet Projections

Given the full discrete operator on a fine grid,  $L_{\epsilon\Delta}$  in Fig. 1, we wish to find an operator of lower dimension that extracts only the coarse scales of the solution. Let  $V_j$  and  $W_j$  refer to the usual scaling and wavelet spaces of some orthogonal wavelet system. Then, for a solution in  $V_{j+1} = V_j \oplus W_j$ , the coarse scale is represented by  $V_j$ , and we are thus interested in the operator that yields the solution's projection onto  $V_j$ . We shall here denote the finite dimensional operator  $L_{\epsilon\Delta}$  by  $L_{j+1}$  in order to indicate scale.

Consider the equation

$$L_{j+1}U = F, \quad U, F \in V_{j+1}, \quad (12)$$

originating from a discretization of a differential equation (1), where  $U$  approximates the solution to the continuous problem. We introduce the orthogonal transformation

$$\mathcal{W}_j : V_{j+1} \rightarrow W_j \times V_j, \quad \mathcal{W}_j U \equiv \begin{pmatrix} U_f \\ U_c \end{pmatrix} \quad U_f \in W_j, \quad U_c \in V_j, \quad (13)$$

and note that the linear operator  $\mathcal{W}_j L_{j+1} \mathcal{W}_j^*$  can be decomposed into four operators acting between the subspaces  $V_j$  and  $W_j$ , such that (12) becomes

$$\begin{pmatrix} A_j & B_j \\ C_j & L_j \end{pmatrix} \begin{pmatrix} U_f \\ U_c \end{pmatrix} = \begin{pmatrix} F_f \\ F_c \end{pmatrix}, \quad U_f, F_f \in W_j, \quad U_c, F_c \in V_j. \quad (14)$$

when we apply  $\mathcal{W}_j$  from the left. Block Gaussian elimination now gives an equation for  $U_c$ , the coarse part of the solution,

$$\bar{L}_j U_c = \bar{F}_j, \quad \bar{L}_j = L_j - C_j A_j^{-1} B_j, \quad \bar{F}_j = F_c - C_j A_j^{-1} F_f. \quad (15)$$

Hence, our new ‘‘coarse grid operator’’  $\bar{L}_j$  is the Schur complement of  $\mathcal{W}_j L_{j+1} \mathcal{W}_j^*$ . We also get the homogenized right hand side,  $\bar{F}_j$ .

For higher dimensions, a standard tensor product extension of the multiresolution analysis allows us to use essentially the same derivation as above to obtain coarse grid operators.

Before we go on, we should note that in general  $\bar{L}_j$  will not be sparse even if  $L_{j+1}$  is, because of the inverse  $A_j^{-1}$ . For the method to be efficient we must be able to approximate  $\bar{L}_j$  with a *sparse* matrix. In Sect. 3.3 below we will get back to this issue and show in subsequent sections that this can indeed be done. The homogenization procedure can be applied recursively on  $\bar{L}_j$  to get  $\bar{L}_{j-1}$  and so on.

The great advantage of this procedure in deriving subgrid models is its generality. It can be used on any system of differential equations and does not require separation into the distinct  $\mathcal{O}(\varepsilon)$  and  $\mathcal{O}(1)$  scales or periodic coefficients. It can also be used to test if it is physically reasonable to represent the effect of fine scales on a coarse scale grid with a local operator.

This work is based on [2,39] and is a continuation of the work by Dorobantu and Engquist, [14]. The original ideas are from Beylkin and Brewster, [6]. See also [21] for analysis in the one-dimensional case.

## 2 Background Theory

In this section we shall present some background material that is helpful in understanding the ideas behind the wavelet homogenization. Most of the material is well known or has at least appeared in the literature. However, the sections on projection generated homogenization and how it relates to classical homogenization are new.

### 2.1 Direct Discretization

Let us first consider the simple approach of using a coarse grid even if not all scales of the original differential equation are clearly resolved. Ideally the following result should be valid,

$$\lim_{h \rightarrow 0} \left( \sup_{\varepsilon < \varepsilon_0} \|u_\varepsilon - u_{\varepsilon, \Delta}\| \right) = 0, \quad (16)$$

where  $h$  is a measure of the element size of or step size in the discretization  $\Delta$ . A convergence result of the form (16) is rarely valid. One example of a problem is the typical error in phase velocity, which most finite element and finite difference methods produce. If  $h$  is not small compared to  $\varepsilon$ , oscillatory parts of a solution

will propagate with  $\mathcal{O}(1)$  errors. There are, however, a few problems for which a weaker version of (16) is valid.

For solutions which are highly oscillatory relative to the grid discretization, numerical techniques without phase velocity errors are needed. In [17,18] particle schemes or method of characteristics approximations of hyperbolic partial differential equations are analyzed. For a restricted class of schemes it is possible to prove convergence, or weak convergence, in  $L^p$  of the numerical approximation to the analytic solution as  $h \rightarrow 0$  essentially independent of  $\varepsilon$ . *Convergence essentially independent of  $\varepsilon$*  means that a set of ratios of  $h/\varepsilon$  with an arbitrary small Lebesgue measure must be excluded to avoid resonance, see [17,18].

One simple but typical example for which a rigorous theory is possible is the method of characteristics for the Carleman equations,

$$\begin{aligned} \frac{\partial u}{\partial t} + \frac{\partial u}{\partial x} + u^2 - v^2 &= 0, & u(x, 0) &= a(x, x/\varepsilon), \\ \frac{\partial v}{\partial t} - \frac{\partial v}{\partial x} + v^2 - u^2 &= 0, & v(x, 0) &= b(x, x/\varepsilon), \end{aligned} \quad (17)$$

where  $a(x, y)$  and  $b(x, y)$  are 1-periodic in  $y$  and the numerical approximation is given by

$$\begin{aligned} u_j^{n+1} &= u_{j-1}^n + \Delta t [(v_{j-1}^n)^2 - (u_{j-1}^n)^2], & u_j^0 &= a(x_j, x_j/\varepsilon), \\ v_j^{n+1} &= v_{j+1}^n + \Delta t [(u_{j+1}^n)^2 - (v_{j+1}^n)^2], & v_j^0 &= b(x_j, x_j/\varepsilon), \end{aligned} \quad (18)$$

with

$$x_j = j\Delta x, \quad t_n = n\Delta t, \quad \Delta t = \Delta x, \quad u(x_j, t_n) \sim u_j^n. \quad (19)$$

The homogenization theory of Tartar, [43], applies to the differential equations (17) and is also used in the convergence proof. The local truncation errors are large for  $h > \varepsilon$  and a cancelation of the errors must be established. The theorem gives strong convergence in  $L^\infty$  essentially independent of  $\varepsilon$  as  $h \rightarrow 0$ .

The wavelet based type of homogenization was derived in order to handle wider classes of differential equations.

## 2.2 Comments on Classical Homogenization

Classical homogenization was briefly described in Sect. 1.1. We shall give a few more results here.

The homogenized coefficient in (10),

$$\hat{G} = \int_{I_d} G(y) - G(y) \frac{d\chi(y)}{dy} dy, \quad (20)$$

consists of two parts. One corresponds to the arithmetic average of the coefficients  $G(y)$ :  $\int_{I_d} G(y) dy$ . The other,

$$\int_{I_d} G(y) \frac{d\chi(y)}{dy} dy, \quad (21)$$

compensates for the effect the high frequency interaction has on the lower frequencies in the solution. The high frequency interaction originates from the product

$G(x/\varepsilon)\nabla u_\varepsilon$ . We have the analogous decomposition of the numerically homogenized operator, see Sect. 2.4.

A rigorous convergence theory can be established for analytic homogenization, [5], and a typical result for the multidimensional problem in Sect. 1.1 with Dirichlet boundary conditions would be,

$$u_\varepsilon \rightharpoonup \bar{u}, \quad \text{weakly in } H_0^1(\Omega), \quad (22)$$

if  $G \in L^\infty(\Omega)$  is 1-periodic,

$$u^T G(y)u \geq \delta |u|^2, \quad \delta > 0, \quad \text{a.e. in } I_d, \quad (23)$$

and  $\Omega \subset \mathbb{R}^d$  is a bounded open domain.

Analytic homogenization extends to coefficients of the form  $G(x, x/\varepsilon)$ . In this case the cell problem with the coefficients  $G(x, y)$  has to be solved for each  $x \in \Omega$ . See [15] for a practical application in the field of oil reservoir modeling.

The derivation of the homogenized operator is traditionally done from an asymptotical assumption on the solution, [5],

$$u_\varepsilon(x) = \bar{u}(x) + \varepsilon u_1(x, x/\varepsilon) + \varepsilon^2 u_2(x, x/\varepsilon) + \mathcal{O}(\varepsilon^3), \quad (24)$$

where  $u_1$  and  $u_2$  are 1-periodic in its second set of arguments. The variables for the different scales  $x$  and  $y = x/\varepsilon$ , are treated independently in the derivation.

The techniques discussed here extends to other cases, including multiple scales where  $G = G(x, x/\varepsilon_1, x/\varepsilon_2, \dots)$ . The homogenization is then applied recursively starting from the smallest scale. However, there has to be a set of distinct scales.

### 2.3 Projection Generated Homogenization

In this section we describe the following approach to homogenization. Consider an equation  $Lu = f$  where  $L$  is a linear operator,  $f$  a right hand side and  $u$  a solution that contains fine scales. Let  $P$  be a projection operator onto a subspace where the fine scales in the original solution do not exist. Our objective is to find the (projection generated) *homogenized* operator  $\bar{L}$  such that  $\bar{L}Pu = f$  for all  $f$  such that  $Pf = f$ . (When  $Pf \neq f$  we also need to find the homogenized right hand side  $\bar{f}$ .) Here, we confine ourselves to the case of Hilbert spaces.

Let  $X$  be a Hilbert space of functions, typically a Sobolev space. Let  $X_0 \subset X$  be a closed subspace representing the coarse part of the functions, and denote by  $P$  the orthogonal (and symmetric) projection operator in  $X$  onto  $X_0$ . Let the spaces  $X_0$  and  $X_0^\perp$  inherit the innerproduct and norm of  $X$ , so that  $\|u\|_X = \|u\|_{X_0}$  when  $u \in X_0$ , and similar for  $X_0^\perp$ . In addition, set  $Q = I - P$  where  $I$  is the identity operator in  $X$ , and introduce the unitary operator  $\mathcal{W}$  on  $X$  defined by

$$\mathcal{W} : X \mapsto X_0 \times X_0^\perp, \quad \mathcal{W}u = \begin{pmatrix} Qu \\ Pu \end{pmatrix}. \quad (25)$$

Let  $\mathcal{L}(X, Y)$  be the set of bounded linear maps from  $X$  to  $Y$ . In the numerical finite dimensional case  $L \in \mathcal{L}(X, Y)$  with  $X = Y = \mathbb{R}^n$ . On order to simplify the presentation we shall consider  $X = Y$  also in infinite dimensions. This means



that partial differential operators will be defined by a special weak formulation, see Remark 1 in Sect. 2.4. For an arbitrary operator  $L \in \mathcal{L}(X, X)$ , we have

$$\begin{aligned} \mathcal{W}L\mathcal{W}^* \begin{pmatrix} u \\ v \end{pmatrix} &= \mathcal{W}L(P+Q)(u+v) = \begin{pmatrix} QL(P+Q)(u+v) \\ PL(P+Q)(u+v) \end{pmatrix} \\ &= \begin{pmatrix} QL(Pv+Qu) \\ PL(Pv+Qu) \end{pmatrix} \equiv \begin{pmatrix} A & B \\ C & D \end{pmatrix} \begin{pmatrix} u \\ v \end{pmatrix} \end{aligned} \quad (26)$$

where

$$\begin{aligned} A &= QLQ \in \mathcal{L}(X_0^\perp, X_0^\perp), & B &= QLP \in \mathcal{L}(X_0, X_0^\perp), \\ C &= PLQ \in \mathcal{L}(X_0^\perp, X_0), & D &= PLP \in \mathcal{L}(X_0, X_0). \end{aligned} \quad (27)$$

When  $A$  is invertible the following definition can be stated:

**Definition 1.** Suppose  $L \in \mathcal{L}(X, X)$  and  $f \in X$ . When  $A$  in (26, 27) is invertible (one-to-one and onto), we define the *homogenized operator*  $\bar{L} : X_0 \mapsto X_0$  as the Schur complement with respect to the decomposition in (26),

$$\bar{L} = D - CA^{-1}B, \quad (28)$$

and the homogenized right hand side as

$$\bar{f} = Pf - CA^{-1}Qf. \quad (29)$$

We will write  $\bar{L}_{X, X_0}$  and  $\bar{f}_{X, X_0}$  when there is a need to show explicitly between which spaces the homogenization step is made. From Definition 1 we immediately have

**Lemma 1.** Suppose  $Lu = f$ , where  $L \in \mathcal{L}(X, X)$ ,  $u \in X$  and  $f \in X$ . If  $A^{-1}$  exists,

$$\bar{L}Pu = \bar{f}. \quad (30)$$

*Proof.* Since  $Lu = f$  we get

$$\mathcal{W}L\mathcal{W}^*\mathcal{W}u = \mathcal{W}f \quad \Rightarrow \quad \begin{pmatrix} A & B \\ C & D \end{pmatrix} \begin{pmatrix} Qu \\ Pu \end{pmatrix} = \begin{pmatrix} Qf \\ Pf \end{pmatrix}. \quad (31)$$

Moreover, since  $A$  is invertible, this system can be reduced with Gaussian elimination. It yields (30).

Note that  $\bar{L}$  and  $\bar{f}$  do not exist for all elements of  $\mathcal{L}(X, X)$  since  $A^{-1}$  may not exist. For some classes of operators  $A$  is however indeed invertible.

**Proposition 1.** Suppose the operator  $L \in \mathcal{L}(X, X)$  is given by the weak form

$$Lu = f \quad \Leftrightarrow \quad a[u, v] = \langle f, v \rangle, \quad \forall v \in X, \quad (32)$$

where  $a[\cdot, \cdot] : X \times X \mapsto \mathbb{R}$  is a bilinear form. If for some positive constants  $c_1$  and  $c_2$ ,

$$\begin{aligned} a[u, v] &\leq c_1 \|u\|_X \|v\|_X, & \forall u, v \in X, \\ a[Qu, Qu] &\geq c_2 \|Qu\|_X^2, & \forall u \in X, \end{aligned} \quad (33)$$

then  $L$  is well-defined and  $A : X_0^\perp \mapsto X_0^\perp$  is one-to-one and onto.

*Proof.* By the first inequality in (33), the bilinear form  $a[u, v]$  is a bounded linear functional on  $X$  for each fixed  $u$ .  $L$  is then well-defined by the Riesz representation theorem. To show that  $A$  is invertible, we need to prove that for every  $f \in X_0^\perp$  there is a unique  $u \in X_0^\perp$  such that

$$a[u, v] = \langle f, v \rangle, \quad \forall v \in X_0^\perp. \quad (34)$$

This follows from the Lax–Milgram lemma if (33) holds.

Some properties kept by the homogenized operator are surjectivity, symmetry and ellipticity, as seen by this proposition.

**Proposition 2.** *Let  $L \in \mathcal{L}(X, X)$  be such that  $\bar{L}$  exists. If  $L$  is onto,  $\bar{L}$  is onto. If  $L$  is self-adjoint,  $\bar{L}$  is self-adjoint. If  $L$  is self-adjoint and also*

$$c_1 \|u\|_X^2 \leq \langle Lu, u \rangle \leq c_2 \|u\|_X^2, \quad \forall u \in X. \quad (35)$$

for some positive constants  $c_1, c_2$ . Then, for the same constants,

$$c_1 \|v\|_{X_0}^2 \leq \langle \bar{L}v, v \rangle \leq \langle Dv, v \rangle \leq c_2 \|v\|_{X_0}^2, \quad \forall v \in X_0. \quad (36)$$

*Proof.* Suppose  $L$  is onto. For any  $f \in X_0 \subset X$  there exists a  $u \in X$  such that  $Lu = f$ . By Lemma 1 then  $\bar{L}Pu = \bar{f}$ . From (29) we see that  $\bar{f} = f$ , so  $\bar{L}$  is also onto. Let  $L$  be self-adjoint. Then  $\mathcal{W}L\mathcal{W}^*$  is self-adjoint and therefore  $A = A^*$ ,  $D = D^*$  and  $C = B^*$ . When  $A$  is invertible this implies that  $(A^{-1})^* = A^{-1}$ . Hence,  $\bar{L}^* = D^* - B^*(A^{-1})^*C^* = D - CA^{-1}B = \bar{L}$ .

Next, assume (35). Take  $v \in X_0$  and set  $u = -A^{-1}Bv \in X_0^\perp$ . Since  $\mathcal{W}$  is unitary,

$$\begin{aligned} c_1 \|v\|_{X_0}^2 &\leq c_1 \|v + u\|_X^2 \leq \langle L(u + v), (u + v) \rangle = \left\langle \begin{pmatrix} A & B \\ C & D \end{pmatrix} \begin{pmatrix} u \\ v \end{pmatrix}, \begin{pmatrix} u \\ v \end{pmatrix} \right\rangle \\ &= \left\langle \begin{pmatrix} 0 \\ -CA^{-1}B + D \end{pmatrix} v, \begin{pmatrix} -A^{-1}Bv \\ v \end{pmatrix} \right\rangle = \langle \bar{L}v, v \rangle. \end{aligned} \quad (37)$$

This proves the left inequality in (36). Since  $C = B^*$  and  $A^{-1}$  is positive by the positivity of  $L$ , we have for the right inequality

$$\begin{aligned} \langle \bar{L}v, v \rangle &= \langle (D - CA^{-1}B)v, v \rangle = \langle Dv, v \rangle - \langle A^{-1}Bv, Bv \rangle \\ &\leq \langle Dv, v \rangle = \langle Lv, v \rangle \leq c_2 \|v\|_X^2 = c_2 \|v\|_{X_0}^2. \end{aligned} \quad (38)$$

We conclude this section by showing that the homogenization is “independent of the path.”

**Proposition 3.** *Let  $X_0$  and  $X_1$  be two closed subspaces of  $X$ , nested such that  $X_0 \subset X_1 \subset X$ . Suppose  $L \in \mathcal{L}(X, X)$  is onto and that  $\bar{L}_{X, X_0}$ ,  $\bar{L}_{X, X_1}$  and  $\bar{L}_{X, X_1 X_1, X_0}$  all exist. If  $\bar{L}_{X, X_0}$  is one-to-one, then*

$$\bar{L}_{X, X_0} = \overline{\bar{L}_{X, X_1 X_1, X_0}}, \quad (39)$$

$$\bar{f}_{X, X_0} = \overline{\bar{f}_{X, X_1 X_1, X_0}}. \quad (40)$$

*Proof.* Let  $P_j$  be the projection onto  $X_j$ . Take  $u \in X_0$  and let  $f = \bar{L}_{X,X_0}u \in X_0$ . Since  $L$  is onto, there is a  $w \in X$  such that  $Lw = f$ . By Lemma 1, we have

$$\bar{L}_{X,X_0}P_0w = \bar{f}_{X,X_0}, \quad \bar{L}_{X,X_1}P_1w = \bar{f}_{X,X_1}. \quad (41)$$

Since  $f \in X_0$  we must have  $\bar{f}_{X,X_0} = \bar{f}_{X,X_1} = f$ , by (29). Another application of Lemma 1, then gives

$$\overline{\bar{L}_{X,X_1X_1,X_0}}P_0P_1w = \bar{f}_{X_1,X_0}. \quad (42)$$

Again,  $\bar{f}_{X_1,X_0} = f$  and  $P_0P_1w = P_0w$  since  $X_0 \subset X_1$ . Hence,

$$\bar{L}_{X,X_0}P_0w = \overline{\bar{L}_{X,X_1X_1,X_0}}P_0w = f = \bar{L}_{X,X_0}u. \quad (43)$$

But,  $\bar{L}_{X,X_0}$  is one-to-one so  $P_0w = u$  and since  $u$  was arbitrary, (39) follows. Finally, letting  $f$  be an arbitrary element of  $X$ , there exists a  $u$  such that  $Lu = f$  since  $L$  is onto and by Lemma 1

$$\bar{f}_{X,X_0} = \bar{L}_{X,X_0}Pu = \overline{\bar{L}_{X,X_1X_1,X_0}}Pu = \overline{\bar{f}_{X,X_1X_1,X_0}}. \quad (44)$$

This shows (40).

## 2.4 Relationship Between the Homogenization Approaches

In the elliptic case, there is a striking similarity between the classical homogenized operator in (10) and the the Schur complement in Definition 1, repeated here for convenience,

$$PLP - PLQ(QLQ)^{-1}QLP, \quad (45)$$

$$\nabla \left( \int_{I_d} G(y) dy \right) \nabla - \nabla \left( \int_{I_d} G(y) \frac{d\chi(y)}{dy} dy \right) \nabla. \quad (46)$$

Both are written as the average of the original operator minus a correction term, which is computed in a similar way for both operators. For the analytical case, a local elliptic cell problem is solved to get  $G\partial_y\chi$ , while in the projection case, a positive operator  $A = QLQ$  defined on a subspace is inverted to obtain  $LQA^{-1}B$ . The average over the terms is obtained by integration in the analytical case, and by applying  $P$  in the projection case.

The relationship can be made more precise, and we will illustrate it by considering the one-dimensional case, with the coarse space given by the lowest Fourier modes. Similar results in one dimension have been shown for wavelet bases, see [21,41].

Consider (2) with  $g^\varepsilon = g(x/\varepsilon)$  where  $g \in L^\infty(\mathbb{T})$  is 1-periodic. Let  $X = H^1(\mathbb{T})$  and write  $\langle \cdot, \cdot \rangle$  for the  $H^1$  innerproduct. Define the operator  $L_\varepsilon \in \mathcal{L}(X, X)$  by the weak form of the equations, such that  $L_\varepsilon u_\varepsilon = f$  is equivalent to

$$a[u, v] := \langle g(x/\varepsilon)\partial_x u_\varepsilon, \partial_x v \rangle_{L^2} = \langle f, v \rangle, \quad \forall v \in H^1(\mathbb{T}). \quad (47)$$

We want to compare this with the classically homogenized operator,

$$\hat{g}\langle \partial_x \bar{u}, \partial_x v \rangle_{L^2} = \langle f, v \rangle, \quad \forall v \in H^1(\mathbb{T}), \quad (48)$$

with  $\hat{g}$  given in (8).

We start by introducing a family of  $\varepsilon$ -dependent spaces  $X_0^\varepsilon$  containing bandlimited functions,

$$X_0^\varepsilon = \left\{ u \in L^2(\mathbb{T}) \mid u = \sum_{|k| < 1/2\varepsilon} a_k e^{2\pi i k x}, a_k \in \mathbb{C} \right\}. \quad (49)$$

Those finite-dimensional spaces are closed subspaces of both  $L^2(\mathbb{T})$  and  $H^1(\mathbb{T})$ . The corresponding orthogonal projections are

$$P_\varepsilon u = \sum_{|k| < 1/2\varepsilon} \hat{u}_k e^{2\pi i k x}, \quad \hat{u}_k = \int_0^1 u(x) e^{-2\pi i k x} dx, \quad (50)$$

where  $\hat{u}_k$  is the  $k^{\text{th}}$  Fourier coefficient of  $u(x)$ .

Let us index the remaining operators by  $\varepsilon$  in the obvious way, setting  $Q_\varepsilon = I - P_\varepsilon$  and

$$\bar{L}_\varepsilon = D_\varepsilon - C_\varepsilon A_\varepsilon^{-1} B_\varepsilon. \quad (51)$$

The strategy is now to explicitly construct (51) corresponding to (47) for fixed  $\varepsilon$  and to show that

$$\lim_{\varepsilon \rightarrow 0} \bar{L}_\varepsilon P_\varepsilon u = \bar{L} u \quad \forall u \in H^1(\mathbb{T}), \quad (52)$$

where  $\bar{L}$  is the homogenized operator in the classical case, given by (48). Under some additional assumptions we can then show that the solution we get from solving  $\bar{L}_\varepsilon \bar{u}_\varepsilon = f$  tends to the homogenized solution  $\bar{u}$  strongly in  $H^1$ .

Our notation in this section will be as follows. We let  $y = x/\varepsilon$  and a  $y$ -dependent function seen as a function of  $x$  will be indicated by a superscripted epsilon, hence  $g(x/\varepsilon) = g^\varepsilon(x)$ . A bar above the function denotes its mean value,

$$\bar{g} = \int_0^1 g(x) dx = \hat{g}_0, \quad (53)$$

where  $\hat{g}_0$  is the zeroth Fourier coefficient of  $g$ . We begin by showing some properties of the projections.

**Lemma 2.** *The projections  $P_\varepsilon$  and  $Q_\varepsilon$  commutes with differentiation,*

$$\partial_x P_\varepsilon u = P_\varepsilon \partial_x u, \quad \partial_x Q_\varepsilon u = Q_\varepsilon \partial_x u, \quad \forall u \in H^1(\mathbb{T}). \quad (54)$$

For  $g \in L^2(\mathbb{T})$  and  $\varepsilon = 1/n$  with  $n \in \mathbb{Z}^+$ ,

$$P_\varepsilon g^\varepsilon P_\varepsilon u = \bar{g} P_\varepsilon u, \quad \forall u \in L^2(\mathbb{T}). \quad (55)$$

For  $u \in L^2(\mathbb{T})$ ,

$$\overline{P_\varepsilon u} = \bar{u}. \quad (56)$$

Finally,

$$\|\partial_x Q_\varepsilon u\|_{L^2} \geq \frac{\pi}{\varepsilon} \|Q_\varepsilon u\|_{L^2}. \quad (57)$$

*Proof.* Take  $u \in H^1(\mathbb{T})$  and let  $\{\hat{u}_k\}$  be its Fourier coefficients. Then

$$\begin{aligned} \partial_x P_\varepsilon u &= \partial_x \sum_{|k| < 1/2\varepsilon} \hat{u}_k e^{2\pi i k x} = \sum_{|k| < 1/2\varepsilon} 2\pi i k \hat{u}_k e^{2\pi i k x} \\ &= P_\varepsilon \sum_k 2\pi i k \hat{u}_k e^{2\pi i k x} = P_\varepsilon \partial_x u. \end{aligned} \quad (58)$$

Since  $Q_\varepsilon = I - P_\varepsilon$ , we have shown (54). Moreover,

$$P_\varepsilon g^\varepsilon P_\varepsilon u = P_\varepsilon \sum_{\ell} \sum_{|k| < n/2} \hat{g}_\ell \hat{u}_k e^{2\pi i(k+n\ell)x} = \hat{g}_0 \sum_{|k| < n/2} \hat{u}_k e^{2\pi i k x} = \bar{g} P_\varepsilon u, \quad (59)$$

since  $|k + n\ell| \geq n/2$  when  $\ell \neq 0$  and  $|k| < n/2$ . This proves (55). Next, for  $u \in L^2$ ,

$$\overline{P_\varepsilon u} = \langle P_\varepsilon u, 1 \rangle_{L^2} = \sum_{|k| < 1/2\varepsilon} \hat{u}_k \langle e^{2\pi i k x}, 1 \rangle_{L^2} = \hat{u}_0 = \bar{u}, \quad (60)$$

showing (56). Finally, from (57),

$$\|\partial_x Q_\varepsilon u\|_{L^2}^2 = \sum_{|k| \geq 1/2\varepsilon} 4\pi^2 k^2 \hat{u}_k^2 \geq \frac{\pi^2}{\varepsilon^2} \sum_{|k| \geq 1/2\varepsilon} \hat{u}_k^2 = \frac{\pi^2}{\varepsilon^2} \|Q_\varepsilon u\|_{L^2}^2. \quad (61)$$

By (57), we now have

$$a[u, v] \leq \|g\|_{L^\infty} \|u\|_{H^1} \|v\|_{H^1}, \quad (62)$$

$$a[Q_\varepsilon u, Q_\varepsilon u] \geq \operatorname{ess\,inf}_{x \in \mathbb{T}} |g(x)| \|\partial_x Q_\varepsilon u\|_{L^2}^2 \geq C \operatorname{ess\,inf}_{x \in \mathbb{T}} |g(x)| \|Q_\varepsilon u\|_{H^1}^2, \quad (63)$$

so Proposition 1 shows that  $A_\varepsilon$  is invertible and  $\bar{L}_\varepsilon$  exists for all  $\varepsilon$ . We can then show

**Theorem 1.** *The projection generated homogenized operator  $\bar{L}_\varepsilon$  corresponding to (47) satisfies*

$$\bar{L}_\varepsilon u = (D_\varepsilon - C_\varepsilon A_\varepsilon^{-1} B_\varepsilon) u = P_\varepsilon \bar{L} u, \quad \forall u \in X_0^\varepsilon \quad (64)$$

if  $\varepsilon = 1/n$  and  $n \in \mathbb{Z}^+$ .

*Proof.* By (54) and (55) we have for  $D_\varepsilon$ ,

$$\begin{aligned} \langle D_\varepsilon u, v \rangle &= \langle g^\varepsilon \partial_x P_\varepsilon u, \partial_x P_\varepsilon v \rangle_{L^2} = \langle g^\varepsilon P_\varepsilon \partial_x u, P_\varepsilon \partial_x v \rangle_{L^2} = \langle P_\varepsilon g^\varepsilon P_\varepsilon \partial_x u, \partial_x P_\varepsilon v \rangle_{L^2} \\ &= \bar{g} \langle \partial_x P_\varepsilon u, \partial_x P_\varepsilon v \rangle_{L^2}. \end{aligned} \quad (65)$$

when  $u, v \in H^1(\mathbb{T})$ . For the second part of the operator, the equation  $A_\varepsilon w = B_\varepsilon u$  needs to be solved. Then  $C_\varepsilon A_\varepsilon^{-1} B_\varepsilon u$  is given by  $C_\varepsilon w$ . In this case we can directly write down the expression for  $w$ , namely

$$w(x) = \int_0^x \chi_y \left( \frac{x'}{\varepsilon} \right) \partial_x P_\varepsilon u(x') dx'. \quad (66)$$

where  $\chi$  is the solution to the cell problem (11). It is well-known that  $\chi \in H^1(\mathbb{T})$ . By also using (54, 55, 56) and the fact that  $P_\varepsilon u \in L^\infty(\mathbb{T})$ , we have

$$\|w\|_{L^2} \leq |w|_\infty \leq \langle |\chi_y^\varepsilon|, |\partial_x P_\varepsilon u| \rangle_{L^2} \leq C \|\chi\|_{H^1} \|P_\varepsilon u\|_{H^1}, \quad (67)$$

$$\|\partial_x w\|_{L^2} \leq |\partial_x P_\varepsilon u|_\infty \|\chi_y^\varepsilon\|_{L^2} \leq C |\partial_x P_\varepsilon u|_\infty \|\chi\|_{H^1}, \quad (68)$$

$$w(1) = \overline{\chi_y^\varepsilon \partial_x P_\varepsilon u} = \overline{P_\varepsilon \chi_y^\varepsilon P_\varepsilon \partial_x u} = 0 = w(0). \quad (69)$$

Therefore  $w \in H^1(\mathbb{T})$ . Moreover, by (54) and (55)

$$\partial_x Q_\varepsilon w = \partial_x w - P_\varepsilon \partial_x w = \partial_x w - P_\varepsilon \chi_y^\varepsilon P_\varepsilon \partial_x u = \partial_x w. \quad (70)$$

Now, from (11) it follows that  $g^\varepsilon \chi_y^\varepsilon = g^\varepsilon + c_0$  a.e., where  $c_0$  is a constant. Together with (70) this shows that  $w$  indeed satisfies  $A_\varepsilon w = B_\varepsilon u$ ,

$$\begin{aligned} \langle A_\varepsilon w, v \rangle &= \langle g^\varepsilon \partial_x Q_\varepsilon w, \partial_x Q_\varepsilon v \rangle_{L^2} = \langle g^\varepsilon \chi_y^\varepsilon \partial_x P_\varepsilon u, \partial_x Q_\varepsilon v \rangle_{L^2} \\ &= \langle g^\varepsilon \partial_x P_\varepsilon u, \partial_x Q_\varepsilon v \rangle_{L^2} + c_0 \langle \partial_x P_\varepsilon u, \partial_x Q_\varepsilon v \rangle_{L^2} \\ &= \langle B_\varepsilon u, v \rangle + c_0 \langle P_\varepsilon \partial_x u, Q_\varepsilon \partial_x v \rangle_{L^2} = \langle B_\varepsilon u, v \rangle. \end{aligned} \quad (71)$$

Then, finally,

$$\begin{aligned} \langle C_\varepsilon A_\varepsilon^{-1} B_\varepsilon u, v \rangle &= \langle C_\varepsilon w, v \rangle = \langle g^\varepsilon \partial_x Q_\varepsilon w, \partial_x P_\varepsilon v \rangle_{L^2} = \langle g^\varepsilon \chi_y^\varepsilon \partial_x P_\varepsilon u, \partial_x P_\varepsilon v \rangle_{L^2} \\ &= \langle P_\varepsilon g^\varepsilon \chi_y^\varepsilon P_\varepsilon \partial_x u, P_\varepsilon \partial_x v \rangle_{L^2} = \overline{g \chi_y} \langle \partial_x P_\varepsilon u, \partial_x P_\varepsilon v \rangle_{L^2}, \end{aligned} \quad (72)$$

which gives

$$\langle D_\varepsilon - C_\varepsilon A_\varepsilon^{-1} B_\varepsilon u, v \rangle = (\bar{g} - \overline{g \chi_y}) \langle \partial_x P_\varepsilon u, \partial_x P_\varepsilon v \rangle_{L^2} = \langle \bar{L} P_\varepsilon u, P_\varepsilon v \rangle. \quad (73)$$

Eventhough both  $\bar{L}$  and  $\bar{L}_\varepsilon$  are well-defined, neither  $\bar{L}$  nor  $\bar{L}_\varepsilon$  are one-to-one on the spaces we have chosen. We need to restrict the operators to smaller spaces on which they are invertible. Let  $X' = H_0^1(0, 1)$  and identify it as a closed subspace of  $H^1(\mathbb{T})$  in the theorem below. On this space  $\bar{L}$  is bounded and positive by Poincaré's inequality,  $\langle \bar{L}u, u \rangle \geq \delta \|u\|_X^2$ . Since  $\bar{L}_\varepsilon = P_\varepsilon \bar{L} P_\varepsilon$  by Theorem 1, this implies (74) and (75). Hence, there are unique solutions  $\bar{u}_\varepsilon$  and  $\bar{u}$  satisfying (76) for  $f \in X_0^\varepsilon$  by the Lax–Milgram lemma. Moreover, Parseval's equality ensures that (77) and (78) hold, since  $P_\varepsilon' u = P_\varepsilon u - (P_\varepsilon u)(0)$  here. The theorem then shows that a solution of  $\bar{L}_\varepsilon \bar{u}_\varepsilon = f$  converges strongly in  $H_0^1(0, 1)$  to the classically homogenized solution when  $\varepsilon \rightarrow 0$ .

**Theorem 2.** *Suppose  $X'$  is a closed subspace of  $X$  such that*

$$\langle \bar{L}_\varepsilon u, u \rangle \geq \delta \|u\|_X^2, \quad \forall u \in X' \cap X_0^\varepsilon, \quad (74)$$

$$\langle \bar{L}_\varepsilon u, v \rangle \leq C \|u\|_X \|v\|_X, \quad \forall u, v \in X_0^\varepsilon. \quad (75)$$

If

$$\bar{L}\bar{u} = f = \bar{L}_\varepsilon \bar{u}_\varepsilon, \quad \bar{u} \in X', \quad \bar{u}_\varepsilon \in X' \cap X_0^\varepsilon, \quad (76)$$

$$\|(\bar{L}_\varepsilon P_\varepsilon - \bar{L})u\|_X \rightarrow 0, \quad u \in X', \quad (77)$$

and with  $P_\varepsilon'$  the orthogonal projection on  $X' \cap X_0^\varepsilon$ ,

$$\|P_\varepsilon' u - u\|_X \rightarrow 0, \quad \|P_\varepsilon u - u\|_X \rightarrow 0, \quad \forall u \in X'. \quad (78)$$

Then

$$\|\bar{u} - \bar{u}_\varepsilon\|_X \rightarrow 0. \quad (79)$$

*Proof.* By (74), for all  $u \in X' \cap X_0^\varepsilon$ ,

$$\|u\|_X^2 \leq \frac{1}{\delta} \langle \bar{L}_\varepsilon u, u \rangle \leq \frac{1}{\delta} \|\bar{L}_\varepsilon u\|_X \|u\|_X. \quad (80)$$

So,

$$\|u\|_X \leq \frac{1}{\delta} \|\bar{L}_\varepsilon u\|_X, \quad \forall u \in X' \cap X_0^\varepsilon. \quad (81)$$

Also, by (75),

$$\|\bar{L}_\varepsilon u\|_X^2 = \langle \bar{L}_\varepsilon u, \bar{L}_\varepsilon u \rangle \leq C \|u\|_X \|\bar{L}_\varepsilon u\|_X \quad \Rightarrow \quad \|\bar{L}_\varepsilon u\|_X \leq C \|u\|_X^2, \quad (82)$$

for all  $u \in X_0^\varepsilon$ . Now, since  $\bar{u}_\varepsilon \in X' \cap X_0^\varepsilon$ ,

$$\begin{aligned} \|\bar{u} - \bar{u}_\varepsilon\|_X &\leq \|P'_\varepsilon \bar{u} - \bar{u}\|_X + \|P'_\varepsilon(\bar{u} - \bar{u}_\varepsilon)\|_X \\ &\leq \|P'_\varepsilon \bar{u} - \bar{u}\|_X + \frac{1}{\delta} \|\bar{L}_\varepsilon P'_\varepsilon(\bar{u} - \bar{u}_\varepsilon)\|_X \\ &\leq \|P'_\varepsilon \bar{u} - \bar{u}\|_X + \frac{1}{\delta} \|(\bar{L}_\varepsilon P_\varepsilon - \bar{L})\bar{u}\|_X + \frac{1}{\delta} \|\bar{L}_\varepsilon(P'_\varepsilon - P_\varepsilon)\bar{u}\|_X \\ &\leq \|P'_\varepsilon \bar{u} - \bar{u}\|_X + \frac{1}{\delta} \|(\bar{L}_\varepsilon P_\varepsilon - \bar{L})\bar{u}\|_X + \frac{C}{\delta} \|(P'_\varepsilon - P_\varepsilon)\bar{u}\|_X \\ &\leq C \|P'_\varepsilon \bar{u} - \bar{u}\|_X + \frac{1}{\delta} \|(\bar{L}_\varepsilon P_\varepsilon - \bar{L})\bar{u}\|_X + \frac{C}{\delta} \|P_\varepsilon \bar{u} - \bar{u}\|_X, \end{aligned} \quad (83)$$

where (76) and (82) were also used. By (77) and (78) the remaining terms vanish.

*Remark 1.* The right hand side  $f$  in (47) does not agree with the right hand side  $\tilde{f}$  of the standard weak formulation of the problem,

$$\langle g(x/\varepsilon) \partial_x u_\varepsilon, \partial_x v \rangle_{L^2} = \langle \tilde{f}, v \rangle_{L^2}, \quad \forall v \in H^1(\mathbb{T}). \quad (84)$$

because of the differences in innerproducts. In fact, in the general standard formulation  $\tilde{f} \in X^* = H^{-1}(\mathbb{T})$  but in order to stay in the framework of Sect. 2.3 we want the range of  $L_\varepsilon$  to be  $X$ . The right hand sides are related by the isomorphic Riesz mapping  $\mathcal{A} : X^* \mapsto X$  such that  $f = \mathcal{A}\tilde{f}$ .

### 3 Wavelet Based Homogenization

In this section we show how the projection generated homogenization works when we choose wavelet spaces as our coarse and fine space decomposition. We start by reviewing the theory of multiresolution analysis. We then let  $Lu = f$  be a finite-dimensional approximation of a partial differential equation and apply the machinery in Sect. 2.3 for this case. In particular, we demonstrate how the resulting  $\bar{L}$  can be approximated by a sparse matrix and used for computing an approximate solution to the differential equation on a coarse grid.

#### 3.1 Multiresolution Analysis

In this section we give a brief outline of the homogenization spaces that we will use. In general we want to homogenize to a subspace that represents the coarse scales of a function space. Therefore, it is close at hand to consider *multiresolution analysis* (MRA) and its related wavelet spaces. A wavelet representation lends itself naturally to analyzing the fine and coarse scales as well as the localization properties of a function. Here we restrict our attention to orthogonal MRA, to align with the theory in Sect. 2.3. The theory could easily be modified to allow also biorthogonal MRA. For a detailed description of MRA we refer the reader to e.g. the book by Daubechies, [13].

An MRA is made up of a ladder of closed function spaces,

$$\dots \subset V_j \subset V_{j+1} \subset \dots, \quad (85)$$

satisfying

$$\overline{\bigcup_{j \in \mathbb{Z}} V_j} = L^2(\mathbb{R}), \quad \bigcap_{j \in \mathbb{Z}} V_j = \{0\}. \quad (86)$$

Moreover, the spaces  $V_j$  represent different scales in the sense that

$$f(x) \in V_j \Leftrightarrow f(2^{-j}x) \in V_0. \quad (87)$$

The zero space should also be invariant under integer translations,

$$f(x) \in V_0 \Rightarrow f(x - k) \in V_0, \quad \forall k \in \mathbb{Z}, \quad (88)$$

and there should exist a *shape function*,  $\varphi \in V_0$ , such that

$$\{\varphi(x - k); k \in \mathbb{Z}\}, \quad (89)$$

is an orthonormal basis for  $V_0$ .

From the MRA definition above follows a number of important properties. Dilates and translates of the shape function form orthonormal bases for the  $V_j$  spaces,

$$\{\varphi_{j,k}(x) = 2^{j/2} \varphi(2^j x - k); k \in \mathbb{Z}\} \text{ is an orthonormal basis for } V_j. \quad (90)$$

Denote the orthogonal complement of  $V_j$  in  $V_{j+1}$  by  $W_j$ ,

$$V_{j+1} = V_j \oplus W_j, \quad V_j \perp W_j. \quad (91)$$

Then,  $L^2(\mathbb{R}) = \overline{\bigoplus_{j \in \mathbb{Z}} W_j}$  and there exists a *mother wavelet*,  $\psi \in W_0$ , with properties corresponding to that of  $\varphi$ ,

$$\{\psi_{j,k}(x) = 2^{j/2} \psi(2^j x - k); k \in \mathbb{Z}\} \text{ is an orthonormal basis for } W_j. \quad (92)$$

This mother wavelet can be constructed explicitly from a given MRA. Note also that  $\{\psi_{j,k}; j, k \in \mathbb{Z}\}$  is an orthonormal basis for  $L^2(\mathbb{R})$ .

An important property of the wavelet  $\psi$  is its number of vanishing moments, i.e. the highest number  $M$  such that

$$\int_{\mathbb{R}} x^k \psi(x) dx = 0, \quad k = 0, \dots, M - 1. \quad (93)$$

This number is related to the wavelet system's approximation qualities. If  $W_j$  is orthogonal to higher degree polynomials,  $V_j$  better approximates smooth functions.

The simplest MRA is the one built on the Haar basis. It has  $M = 1$  and the shape function and the mother wavelet are given by

$$\varphi(x) = \begin{cases} 1, & \text{if } 0 \leq x \leq 1, \\ 0, & \text{otherwise,} \end{cases} \quad \psi(x) = \begin{cases} 1, & \text{if } 0 \leq x \leq 1/2, \\ -1, & \text{if } 1/2 < x \leq 1, \\ 0, & \text{otherwise.} \end{cases} \quad (94)$$



In more than one dimension, the MRA is extended by considering tensor product spaces. Each dimension can be treated separately, using the one-dimensional analysis. The resulting multi-dimensional MRA is a tensor product of one-dimensional MRAs. In two dimensions, we define the tensor product spaces

$$\mathbf{V}_j = V_j \otimes V_j, \quad \dots \subset \mathbf{V}_j \subset \mathbf{V}_{j+1} \subset \dots, \quad j \in \mathbb{Z}, \quad (95)$$

with  $V_j$  being the one-dimensional spaces introduced above. The spaces  $\mathbf{V}_j$  will satisfy the same conditions, (85)-(89), as the  $V_j$  spaces, with  $\mathbb{R}, \mathbb{Z}$  replaced by  $\mathbb{R}^2, \mathbb{Z}^2$ . The shape function of this two-dimensional MRA can be written in terms of the one-dimensional shape function,

$$\varphi(\mathbf{x}) = \varphi(x_1) \otimes \varphi(x_2) = \varphi(x_1)\varphi(x_2). \quad (96)$$

It follows, as in the one-dimensional case, that

$$\{\varphi_{j,k,l}(\mathbf{x}) = \varphi_{j,k}(x_1) \otimes \varphi_{j,l}(x_2)\}, \quad k, l \in \mathbb{Z}, \quad (97)$$

is an orthonormal basis for  $\mathbf{V}_j$ . Furthermore, denoting the orthogonal complement of  $\mathbf{V}_j$  in  $\mathbf{V}_{j+1}$  by  $\mathbf{W}_j$ , we have that

$$\mathbf{V}_{j+1} = \mathbf{V}_j \oplus \mathbf{W}_j, \quad \mathbf{V}_j \perp \mathbf{W}_j, \quad L^2(\mathbb{R}^2) = \overline{\bigoplus_{j \in \mathbb{Z}} \mathbf{W}_j}. \quad (98)$$

The wavelet space  $\mathbf{W}_j$  is composed of three parts,

$$\mathbf{W}_j = (W_j \otimes W_j) \oplus (V_j \otimes W_j) \oplus (W_j \otimes V_j). \quad (99)$$

Here, the  $W_j$  spaces are those of the one-dimensional case, given by (91). Similar tensor product extensions can be made also for higher dimensions.

### 3.2 Wavelet Projections of Difference Operators

We will now discuss homogenization in a more concrete setting. The spaces we use are the finite dimensional wavelet spaces discussed in Sect. 3.1. The typical operators that we homogenize are discrete approximations of differential operators. As seen above in Sect. 2.3, given such an operator, defined on a fine grid, the idea of projection generated homogenization is to find an operator defined on a smaller space that extracts only the coarse scales of the solution. For a function in the wavelet space  $V_{j+1}$ , the coarse scale is represented by  $V_j$ , and we are in the first step thus interested in the homogenized operator given by  $\bar{L}_{V_{j+1}, V_j}$ . We will mostly use the standard Haar basis.

Let us now consider the equation

$$L_{j+1}U = F, \quad U, F \in V_{j+1}, \quad L_{j+1} \in \mathcal{L}(V_{j+1}, V_{j+1}). \quad (100)$$

This equation may originate from a finite difference, finite element or finite volume discretization of a given differential equation. In the Haar case  $U$  can be identified as a piecewise constant approximation of  $u(x)$ , the solution to the continuous problem. Let  $\mathcal{W}_j : V_{j+1} \mapsto V_j \times W_j$  be the unitary operator corresponding to (25). (By (91)

$V_j^\perp = W_j$ .) As in the infinite dimensional case (31), we apply the transformation  $\mathcal{W}_j$  on  $L_{j+1}$  from the left and get

$$\mathcal{W}_j L_{j+1} \mathcal{W}_j^* (\mathcal{W}_j U) = \mathcal{W}_j F \quad (101)$$

or if we decompose  $\mathcal{W}_j L_{j+1} \mathcal{W}_j^*$  according to (26),

$$\begin{pmatrix} A_j & B_j \\ C_j & L_j \end{pmatrix} \begin{pmatrix} U_f \\ U_c \end{pmatrix} = \begin{pmatrix} F_f \\ F_c \end{pmatrix}, \quad U_f, F_f \in W_j, \quad U_c, F_c \in V_j. \quad (102)$$

Here the subindex ‘‘f’’ means projection onto the fine scale subspace,  $W_j$  in this case, and subindex ‘‘c’’ stands for projection onto the coarse scale subspace,  $V_j$  here. This is a convention we will use frequently. Also note that we changed the notation of the block previously called  $D_j$  to  $L_j$ , to indicate that  $L_j = PL_{j+1}P$  actually corresponds to one type of direct discretization on the coarse scale.

The homogenized ‘‘coarse grid operator’’ is now given by block Gaussian elimination of (102),

$$(L_j - C_j A_j^{-1} B_j) U_c = F_c - C_j A_j^{-1} F_f. \quad (103)$$

For simplicity we will use the notation  $\overline{L}_{j+1, V_{j+1}, V_j} \equiv \bar{L}_j$  and  $\overline{F}_{V_{j+1}, V_j} \equiv \bar{F}_j$ . Hence,

$$\bar{L}_j = L_j - C_j A_j^{-1} B_j, \quad \bar{F}_j = F_c - C_j A_j^{-1} F_f. \quad (104)$$

Since  $L_j$  corresponds to a direct coarse discretization, we can interpret  $C_j A_j^{-1} B_j$  as a correction term, which includes subgrid phenomena in  $\bar{L}_j$ .

In the finite dimensional case, we will represent the operators using their matrix representations with respect to the bases given by (90) and (92). For instance in the Haar basis, we get the following matrix representation of  $\mathcal{W}_j$ ,

$$\mathcal{W}_j = \begin{pmatrix} \bar{Q}_j \\ \bar{P}_j \end{pmatrix} = \frac{1}{\sqrt{2}} \begin{pmatrix} 1 & -1 & 0 & \cdots & & \\ 0 & 0 & 1 & -1 & 0 & \cdots \\ \vdots & \vdots & \vdots & \vdots & \vdots & \vdots \\ 0 & 0 & \cdots & 0 & 1 & -1 \\ 1 & 1 & 0 & \cdots & & \\ 0 & 0 & 1 & 1 & 0 & \cdots \\ \vdots & \vdots & \vdots & \vdots & \vdots & \vdots \\ 0 & 0 & \cdots & 0 & 1 & 1 \end{pmatrix}. \quad (105)$$

Note, in this representation  $\bar{P}_j^*$  and  $\bar{Q}_j^*$  are bases in  $V_{j+1}$  for  $V_j$  and  $W_j$ , respectively. The corresponding projections in  $V_{j+1}$  are  $\bar{P}_j^* \bar{P}_j$  and  $\bar{Q}_j^* \bar{Q}_j$ . The matrix representation of (102) is a block matrix decomposition of the same form as the operator decomposition.

Before we go on we should also note that in general  $\bar{L}_j$  will not be represented by a sparse matrix even if  $L_{j+1}$  is, because  $A_j^{-1}$  would typically be dense. For the homogenization method to be efficient we must be able to approximate  $\bar{L}_j$  with a sparse matrix. If this sparse matrix is on banded form, it can be seen as a discretization of a local differential operator acting on the coarse space. In Sect. 3.3 we will get back to this issue and in subsequent sections we will show that this can indeed be done for many applications.

The procedure to obtain  $\bar{L}_j$  described above can be applied recursively on  $\bar{L}_j$  itself to get  $\bar{L}_{j-1}$  and so on. This can easily be verified when  $L_{j+1}$  is symmetric positive definite. Then  $A_j$  is always invertible by Proposition 1 (with  $a[u, v] = \langle Lu, v \rangle$ ) and Proposition 2 shows that also  $\bar{L}_j$  is symmetric positive definite. By

induction  $\bar{L}_k$  exists for  $k \leq j$ . Also note that Proposition 3 gives  $\bar{L}_k = \overline{L_{j+1}}_{V_{j+1}, V_k}$  and  $\bar{F}_k = \bar{F}_{V_{j+1}, V_k}$  for  $k \leq j$ .

Moreover, an improvement in the condition number can often be estimated. Typically for standard discretizations

$$\max_{\|v\|=1} \langle L_k v, v \rangle < \max_{\|u\|=1} \langle L_{j+1} u, u \rangle, \quad (106)$$

when  $k \leq j$ . Then, from Proposition 2,

$$\begin{aligned} \kappa(\bar{L}_k) &= \frac{\max_{\|v\|=1} \langle \bar{L}_k v, v \rangle}{\min_{\|v\|=1} \langle \bar{L}_k v, v \rangle} < \frac{\max_{\|v\|=1} \langle L_k v, v \rangle}{\min_{\|v\|=1} \langle L_{j+1} v, v \rangle} \\ &< \frac{\max_{\|v\|=1} \langle L_{j+1} v, v \rangle}{\min_{\|v\|=1} \langle L_{j+1} v, v \rangle} = \kappa(L_{j+1}). \end{aligned} \quad (107)$$

The two-dimensional wavelet transform

$$\mathcal{W}_j : \mathbf{V}_{j+1} \mapsto \mathbf{W}_j \times \mathbf{V}_j \quad (108)$$

can be written as a tensor product of one-dimensional transforms,

$$\mathcal{W}_j = \mathcal{W}_j \otimes \mathcal{W}_j. \quad (109)$$

A linear operator  $L_{j+1}$  that acts on the space  $\mathbf{V}_{j+1}$  can be decomposed in a way similar to the one-dimensional case. The equation

$$L_{j+1}U = F, \quad U, F \in \mathbf{V}_{j+1}, \quad L_{j+1} \in \mathcal{L}(\mathbf{V}_{j+1}, \mathbf{V}_{j+1}) \quad (110)$$

can then be transformed to

$$\begin{pmatrix} A_j & B_j \\ C_j & L_j \end{pmatrix} \begin{pmatrix} U_f \\ U_c \end{pmatrix} = \begin{pmatrix} F_f \\ F_c \end{pmatrix}, \quad U_f, F_f \in \mathbf{W}_j, \quad U_c, F_c \in \mathbf{V}_j, \quad (111)$$

and the coarse grid operator is again the Schur complement,

$$\bar{L}_{V_{j+1}, V_j} \equiv \bar{L}_j = L_j - C_j A_j^{-1} B_j. \quad (112)$$

To get the matrix representation of (111), we take the one-dimensional matrix representations of  $\mathcal{W}_j$  and, following (109), compute its Kronecker tensor product with itself. We must thereafter also apply a suitable permutation matrix to the product in order to get the same block structure of the matrix as in (111).

Note that the fine scale part of  $U$  can be decomposed as

$$U_f = \begin{pmatrix} U_{ff} \\ U_{cf} \\ U_{fc} \end{pmatrix}, \quad U_{ff} \in W_j \otimes W_j, \quad U_{cf} \in V_j \otimes W_j, \quad U_{fc} \in W_j \otimes V_j. \quad (113)$$

In some cases, the homogenized operator keeps important properties of the original operator. Let the forward and backward undivided differences be defined as

$$\Delta_+ u_i = u_{i+1} - u_i, \quad \Delta_- u_i = u_i - u_{i-1}. \quad (114)$$

In [14] it was shown that the one-dimensional elliptic model equation  $-(gu')' = f$  discretized with

$$-\Delta_+ \text{diag}(g) \Delta_- U = h^2 F \quad (115)$$

will preserve its divergence form during homogenization. That is, we will get

$$\bar{L}_j = \frac{1}{h^2} \Delta_+ H_j \Delta_-, \quad (116)$$

where  $H_j$  is a strongly diagonal dominant matrix which can be interpreted as the effective material coefficient related to  $g$ . Analogously, for the first order differential operator  $g(x) \frac{\partial}{\partial x}$  the discretized form  $\text{diag}(g) \Delta_- / h$  is preserved during homogenization,

$$\bar{L}_j = \frac{1}{h} H_j \Delta_-. \quad (117)$$

In two dimensions, the elliptic model equation  $-\nabla(g(x, y) \nabla u) = f$  can be discretized as

$$L_{j+1} = -\frac{1}{h^2} \Delta_+^x G \Delta_-^x - \frac{1}{h^2} \Delta_+^y G \Delta_-^y, \quad L_{j+1} U = F. \quad (118)$$

Then  $\bar{L}_j$  is no longer on exactly the same form as  $L_{j+1}$ . The cross-derivatives must also be included. We get

$$\bar{L}_j = -\frac{1}{h^2} \Delta_+^x H^{xx} \Delta_-^x - \frac{1}{h^2} \Delta_+^y H^{yy} \Delta_-^y - \frac{1}{h^2} \Delta_+^x H^{xy} \Delta_-^y - \frac{1}{h^2} \Delta_+^y H^{yx} \Delta_-^x. \quad (119)$$

*Remark 2.* Spaces other than wavelet spaces could also be used. For instance, in the settings described in [29], [34] and [24] the coarse subspace is simply the grid function space given by removing every other grid point. In the classical homogenization setting the solution has the asymptotic expansion (24), as discussed in Sect. 2.2. The techniques mentioned above give homogenized operators with coarse grid solutions which directly samples (24). The oscillatory term  $\varepsilon u_1(x, x/\varepsilon)$  is contained in the solution. In the wavelet homogenization the solution is a projection of  $u_\varepsilon$  onto a coarse scale  $V_j$  space. The influence of the  $u_1$  term, which oscillates with mean zero, [5], is then significantly reduced.

### 3.3 Compact Representation of Projected Operators

When the operator  $L_{j+1}$  is derived from a finite difference, finite element or finite volume discretization, it is sparse and of a certain structure. In one dimension it might, for instance, be tridiagonal. However, as remarked in Sect. 3.2, the matrix  $\bar{L}_j$  is in general not sparse since  $A_j^{-1}$  is usually dense. Computing all components of  $\bar{L}_j$  would be inefficient. Fortunately,  $\bar{L}_j$  will be diagonal dominant in many important cases and we should then be able to find a sparse matrix that is a close approximation of  $\bar{L}_j$ .

In some simple cases the matrix  $A_j$  is in fact diagonal. Examples include operators  $L$  of the form

$$Lu = \int_0^x a(t)u(t)dt + b(x)u(x). \quad (120)$$

Let  $P_j$  be the orthogonal projection on  $V_j$ . Suppose  $L$  is discretized in  $V_{j+1}$  as  $L_{j+1} = P_{j+1} L P_{j+1}$  with  $a$  in (120) replaced by  $P_{j+1} a P_{j+1}$ , and similar for  $b$ . When the Haar system is used,  $A_j$  is diagonal and  $\bar{L}_j$  is of the same form as  $L_{j+1}$ , cf. Chap. 7. Let  $\bar{A}_k$  be related to  $\bar{L}_{k+1}$  via (101, 102) in the same way as  $A_j$  relates to  $L_{j+1}$ . By induction,  $\bar{A}_k$  is also diagonal for  $k < j$ . The operators in (120) turn up for instance in problems with systems of ordinary differential equations and

one-dimensional elliptic equations, see [6,21]. In these cases, an explicit recurrence relation between scale levels can be established, which permits the computation of  $\bar{L}_k$  on any fixed level  $k$  as the starting level,  $j + 1$ , tends to infinity.

For more general problems one must instead rely on the rapid decay of elements in  $A_j$  and  $\bar{L}_j$  off the diagonal, which is a consequence of the wavelet spaces' good approximation properties. The decay rate of  $A_j$  for Calderon–Zygmund and pseudo-differential operators were given by Beylkin, Coifman and Rokhlin in [8]. Letting  $L_{j+1} = P_{j+1}LP_{j+1}$ ,  $A_j = \{a_{k\ell}^j\}$ ,  $B_j = \{b_{k\ell}^j\}$  and  $C_j = \{c_{k\ell}^j\}$ , they show that

$$|a_{k\ell}^j| + |b_{k\ell}^j| + |c_{k\ell}^j| \leq \frac{2^{-\lambda j} C_M}{1 + |k - \ell|^{M+1}}, \quad |k - \ell| \geq \nu, \quad (121)$$

when the wavelet system has  $M$  vanishing moments. For Calderon–Zygmund operators  $\lambda = 0$  and  $\nu = 2M$ . For a pseudo-differential operator  $\nu = 0$  and if its symbol is  $\sigma(x, \xi)$ , the value of  $\lambda$  should be taken such that the estimates

$$|\partial_\xi^\alpha \partial_x^\beta \sigma(x, \xi)| \leq C_{\alpha, \beta} (1 + |\xi|)^{\lambda - \alpha + \beta}, \quad (122)$$

$$|\partial_\xi^\alpha \partial_x^\beta \sigma^*(x, \xi)| \leq C_{\alpha, \beta} (1 + |\xi|)^{\lambda - \alpha + \beta}, \quad (123)$$

are satisfied for some constants  $C_{\alpha, \beta}$ . For instance, in the second order elliptic case  $\lambda = 2$ . Moreover, Beylkin and Coult, [9], showed that if (121) holds with  $\lambda = 0$  for  $A_j$ ,  $B_j$  and  $C_j$  given by  $L_{j+1}$  in (101, 102), then the same estimate also holds for  $\bar{A}_{j'}$ ,  $\bar{B}_{j'}$  and  $\bar{C}_{j'}$ , here given by  $P_{j'} \bar{L}_{k+1} P_{j'}$  for  $j' \leq k < j$  with  $j + 1$  being the starting homogenization level. Hence, the decay rate is preserved after homogenization.

The decay estimate in [9] for  $\bar{A}_{j'}$  is uniform in  $k$  and may not be sharp for a fixed  $k$ . There is, for example, a general result by Concus, Golub and Meurant, [12], for diagonal dominant, symmetric and tridiagonal matrices. For those cases, which include  $A_j$  corresponding to the discretization in (115) of the one-dimensional elliptic operator, the inverse has exponential decay,

$$|(A_j^{-1})_{k\ell}| \leq C \varrho^{|k-\ell|}, \quad 0 < \varrho < 1. \quad (124)$$

This holds also when the elliptic operator has a lower order term of type  $b(x)\partial_x$  discretized with upwinding, [30].

One simple way to approximate  $\bar{L}_j$  is to set all components outside a prescribed bandwidth  $\nu$  equal to zero. Let us define

$$\text{trunc}(M, \nu)_{ij} = \begin{cases} M_{ij}, & \text{if } 2|i - j| \leq \nu - 1 \\ 0, & \text{otherwise.} \end{cases} \quad (125)$$

For  $\nu = 1$  the matrix is diagonal. For  $\nu = 3$  it is a tridiagonal and so on. We thus proceed here in order to control the structure of  $\bar{L}_j$  and we refer to it as *truncation*. For lower triangular matrices we define truncation to lower triangular form as

$$\text{trunc}_L(M, \nu)_{ij} = \begin{cases} M_{ij}, & \text{if } 0 \leq i - j \leq \nu - 1 \\ 0, & \text{otherwise.} \end{cases} \quad (126)$$

Another possible strategy is the basic truncation method used in [8],

$$\text{trunc}_{\text{BCR}}(M, \varepsilon)_{ij} = \begin{cases} M_{ij}, & \text{if } |M_{ij}| > \varepsilon, \\ 0, & \text{otherwise} \end{cases} \quad (127)$$

but it is not practical here since the location of the non-zero elements cannot be controlled. The matrix  $\bar{L}_j$  can also be projected onto banded form in a more effective manner. The aim is that the projected matrix should give the same result as the original matrix on a given subspace, e.g. when applied to vectors representing smooth functions. Let  $\{\mathbf{v}_j\}_{j=1}^\nu$  be a set of linearly independent vectors in  $\mathbb{R}^N$ . Denote the subspace of  $\mathbb{R}^{N \times N}$  with matrices essentially<sup>1</sup> of bandwidth  $\nu$  by  $\mathcal{T}_\nu$ . Moreover, let

$$\mathcal{L}_\nu = \{M \in \mathbb{R}^{N \times N} : \text{span}\{\mathbf{v}_1, \mathbf{v}_2, \dots, \mathbf{v}_\nu\} \subset \mathbf{N}(M)\}, \quad (128)$$

where  $\mathbf{N}(M)$  represents the null space of  $M$ . Then

$$\mathbb{R}^{N \times N} = \mathcal{T}_\nu \oplus \mathcal{L}_\nu \quad (129)$$

and we define the *band projection* of a matrix  $M \in \mathbb{R}^{N \times N}$  as the projection of  $M$  onto  $\mathcal{T}_\nu$  along  $\mathcal{L}_\nu$ , with the notation

$$\text{band}(M, \nu) = \text{Proj}_{\mathcal{T}_\nu} M. \quad (130)$$

As a consequence,

$$M\mathbf{x} = \text{band}(M, \nu)\mathbf{x}, \quad \forall \mathbf{x} \in \text{span}\{\mathbf{v}_1, \mathbf{v}_2, \dots, \mathbf{v}_\nu\}. \quad (131)$$

In our setting  $M$  will usually operate on vectors representing smooth functions, for instance solutions to elliptic equations, and a natural choice for  $\mathbf{v}_j$  vectors are thus the first  $\nu$  polynomials,

$$\mathbf{v}_j = \{1^{j-1}, 2^{j-1}, \dots, N^{j-1}\}^*, \quad j = 1, \dots, \nu. \quad (132)$$

Smooth solutions to the homogenized problem should be well approximated by these vectors. For the case  $\nu = 1$  we get the standard ‘‘masslumping’’ of a matrix, often used in the context of finite element methods.

This technique is similar to the probing technique used by Chan et al., [11]. In that case the vectors  $\mathbf{v}_j$  are sums of unit vectors. Other probing techniques have been suggested by Axelsson, Pohlman and Wittum, see Chapter 8 in [3]. The choice of  $\mathbf{v}_j$  vectors could be optimized if there is some a priori knowledge of the homogenized solution. In some cases the band projection technique only gives improvements for small values of  $\nu$ , see Fig. 2. The probing technique of [11] could be used for larger  $\nu$  in our examples. Numerical evidence indicate that for small values of  $\nu$ , the band projection technique is more efficient.

The focus here is on the principle and the truncation  $\text{trunc}(\bar{L}_j, \nu)$  is done after computing the full inverse of  $A_j$ , which is expensive. By capitalizing on the nearly sparse structure of the matrices involved, it was however shown in [9] that the cost can be reduced to  $\mathcal{O}(N)$  operations for  $N$  unknowns and fixed accuracy. This method uses a multiresolution based LU decomposition procedure described in [10]. Moreover, the same homogenized operator will typically be reused multiple times, for instance with different right hand sides, or in different places of the geometry as a subgrid model. This aspect will be exemplified below in Sect. 5.3 and Sect. 5.4. The

<sup>1</sup> We must require that each row of the matrices in  $\mathcal{T}_\nu$  has the same number of elements. Therefore, the first and last  $\nu - 1$  rows will have additional elements located immediately to the right and left of the band, respectively.

computation of  $\text{band}(\bar{L}_j, \nu)$  can be based on  $\text{trunc}(\bar{L}_j, \mu)$ ,  $\mu > \nu$ . The additional computational cost is proportional to  $(\nu^3 + \mu\nu)N$ . The  $\nu^3 N$  term corresponds to solving  $N$   $\nu \times \nu$  systems and  $\mu\nu N$  to computing the right hand sides, see also [3].

The truncation methods described above are even more efficient when applied to  $H_j$  instead of directly to the homogenized operator. The following proposition shows that when the solution to the homogenized problem belongs to the Sobolev space  $H^1$ , the accuracy is one order higher.

**Proposition 4.** *Suppose  $L = \Delta_+ H \Delta_-$  and  $LU = h^2 f$ . Let  $\kappa = \|L^{-1}\| \cdot \|H\|$  and*

$$r = \frac{\|\delta L\|}{\|L\|} = \frac{\|\delta H\|}{\|H\|} < \frac{1}{4\kappa}, \quad (133)$$

where  $\|\cdot\|$  denotes the  $l_2$ -norm. Furthermore, let  $u$  be any  $H^1$ -function such that  $U_j = u(jh)$ . Then, if

$$(L + \delta L)(U + \delta U_L) = h^2 f, \quad (134)$$

$$\Delta_+(H + \delta H)\Delta_-(U + \delta U_H) = h^2 f \quad (135)$$

the following bounds on the perturbed solutions hold  $\forall f$

$$\|\delta U_L\| \leq \frac{4r\kappa}{1-4r\kappa} \|U\|, \quad (136)$$

$$\|\delta U_H\| \leq \frac{1}{2} \cdot \frac{4r\kappa}{1-4r\kappa} \|\Delta_- U\| \leq \frac{h}{2} \cdot \frac{4r\kappa}{1-4r\kappa} \|u\|_{H^1}. \quad (137)$$

The bound (136) is sharp.

*Proof.* Using  $\|\Delta_+\| = \|\Delta_-\| = 2$  and (133) we have

$$\|L^{-1}\delta L\| \leq \frac{\|L^{-1}\| \cdot \|\delta H\| \cdot \|\Delta_+ H \Delta_-\|}{\|H\|} \leq 4r\|L^{-1}\| \cdot \|H\| = 4r\kappa < 1. \quad (138)$$

Therefore,

$$\|\delta U_L\| = \|(I + L^{-1}\delta L)^{-1} L^{-1}\delta L U\| \leq \frac{\|L^{-1}\delta L\|}{1 - \|L^{-1}\delta L\|} \|U\| \leq \frac{4r\kappa}{1-4r\kappa} \|U\|, \quad (139)$$

proving the first bound. In the second case,

$$\|L^{-1}\Delta_+\delta H\Delta_-\| \leq 4\|L^{-1}\| \cdot \|\delta H\| \leq 4r\kappa < 1, \quad (140)$$

giving

$$\begin{aligned} \|\delta U_H\| &= \|(I + L^{-1}\Delta_+\delta H\Delta_-\)^{-1} L^{-1}\Delta_+\delta H\Delta_- U\| \\ &\leq \frac{\|L^{-1}\Delta_+\delta H\|}{1 - \|L^{-1}\Delta_+\delta H\Delta_-\|} \|\Delta_- U\| \leq \frac{2r\kappa}{1-4r\kappa} \|\Delta_- U\| \end{aligned} \quad (141)$$

which proves the second bound. The choice  $L = -\Delta_+\Delta_-$ ,  $\delta L = -\tau I\|L\|$  and  $f$  the eigenvector of  $L$  corresponding to its smallest eigenvalue shows the sharpness of (136). The final step,  $\|\Delta_- U\| \leq h\|u\|_{H^1}$ , follows from Cauchy-Schwarz's inequality. Note that (136) cannot be improved to  $\mathcal{O}(h)$  by replacing  $\|U\|$  with  $\|u\|_{H^1}$ .

In two dimensions truncation to simple banded form is in general not adequate, since the full operator will typically be block banded. However, both the crude truncation and the band projection generalizes easily to treat block banded form instead of just banded. Let  $M$  be the tensor product of two  $N \times N$  matrices. Then we define truncation as

$$\text{trunc}_2(M, \nu)_{ij} = \begin{cases} M_{ij}, & \text{if } 2|i - j - \tau N| \leq \nu - 1 - |2r|, \\ 0, & \text{otherwise,} \end{cases} \quad |2r| + 1 \leq \nu. \quad (142)$$

This mimics the typical block structure of a discretized differential operator. For the band projection, the space  $\mathcal{T}_\nu$  of banded matrices in the one-dimensional definition, is simply replaced by the space of matrices with the block banded sparsity pattern defined in (142).

In two dimensions, untangling the various  $H$  components of (119) from  $\bar{L}$  is more complicated than finding the  $H$  in (116) and (117) for one-dimensional problems. There is however no unsurmountable difficulty, and truncating  $H$  instead of  $\bar{L}$  can be done also for two-dimensional problems.

## 4 Numerical Examples

In this section we present numerical results for the algorithms described above. Elliptic and hyperbolic model problems are studied. In one of the examples the wavelet based homogenization is applied to the Helmholtz equation for the generation of a course grid approximation. This could potentially be useful for sub grid scale modeling in computational electromagnetics.

### 4.1 Elliptic Problems

Consider first the one-dimensional elliptic model equation,

$$-\frac{d}{dx} \left( g(x) \frac{du}{dx} \right) = f(x), \quad u(0) = u'(1) = 0, \quad (143)$$

with  $g(x) > 0$  and then the Helmholtz equation,

$$-\sum_{i=1}^d \frac{\partial}{\partial x_i} g(x) \frac{\partial u}{\partial x_i} - \omega^2 u(x) = 0, \quad (144)$$

in one and two dimensions ( $d = 1, 2$ ). The Helmholtz equation can be derived from the wave equation  $v_{tt} = \nabla \cdot g(x) \nabla v$  under the assumption that  $v(x, t) = u(x) e^{i\omega t}$ . Hence  $u(x)$  represents the amplitude and  $\omega$  is the frequency.

Uniform finite volume discretization will be used in the numerical experiments. The computational domain is the unit interval (square in 2D). The grid size is denoted  $n$ , and the cell size  $h = 1/n$ . For a function  $u(x)$  the corresponding grid function is written  $u_i$  (or  $u_{ij}$ ). The grid function approximates cell averages,

$$u_i \sim \frac{1}{h} \int_{(i-1)h}^{ih} u(x) dx, \quad i = 1, \dots, n, \quad (145)$$



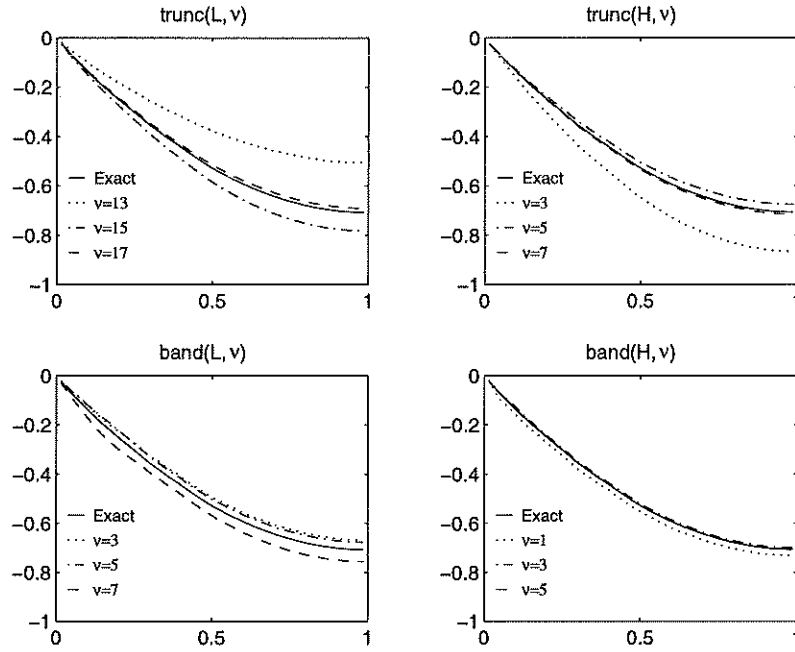


**Fig. 2.** Result for the elliptic model problem,  $g(x)$  random, when the homogenized operator is approximated in different ways. The “exact” solution refers to the solution with the full  $32 \times 32$  homogenized operator

in one dimension and

$$u_{ij} \sim \frac{1}{h^2} \int_{(i-1)h}^{ih} \int_{(j-1)h}^{jh} u(x_1, x_2) dx_1 dx_2, \quad i, j = 1, \dots, n, \quad (146)$$

in two dimensions. The whole vector  $(u_1, \dots, u_n)^T$  will be denoted by  $U$ . In two dimensions,  $U = (u_{11}, \dots, u_{1n}, u_{21}, \dots, u_{2n}, \dots, u_{nn})^T$ .

### The 1D Elliptic Model Equation

We approximate (143) with the discretization

$$-\frac{1}{h^2} \Delta_+ g_i \Delta_- u_i = f_i, \quad i = 1, \dots, n, \quad u_0 = -u_1, \quad u_{n+1} = u_n. \quad (147)$$

First, set  $f = -1$  and let the coefficients of  $g(x)$  have a uniform random distribution in the interval  $[0.5, 1]$ . Take  $n = 256$  and make three homogenization steps. The coarsest level contains 32 grid points.

In Fig. 2 different truncation strategies are compared. The exact reference solution is given by the numerically homogenized operator at the coarsest level without any truncation. This is equivalent to the projection onto the coarse scale of the solution on the finest scale. In the top two subplots we use crude truncation, (125).

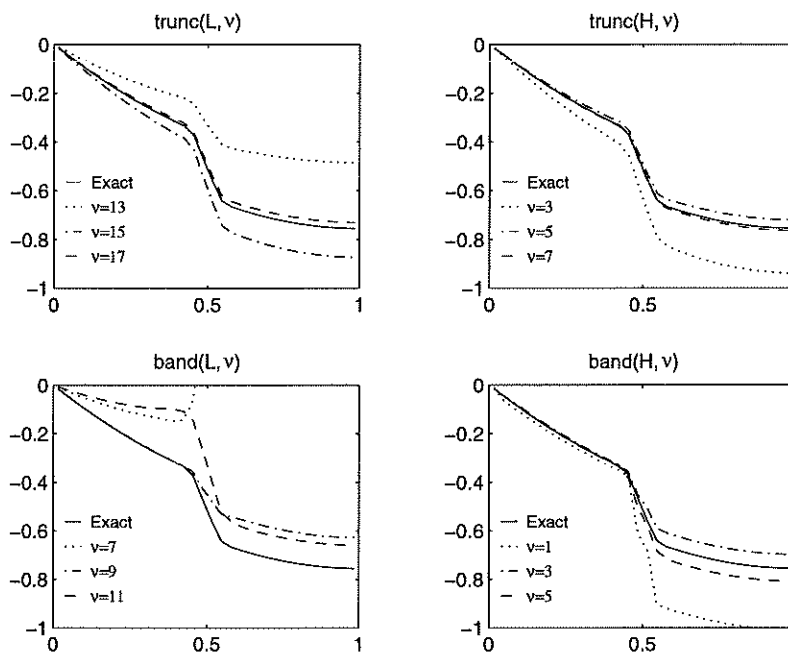


**Fig. 3.** Result for the elliptic model problem,  $g(x)$  a slit, when the homogenized operator is approximated in different ways. The “exact” solution refers to the solution with the full  $32 \times 32$  homogenized operator

In the bottom two subplots we use the band projection described in Sect. 3.3. The approximation is performed on  $H$ , see (116), and on  $\bar{L}$  after all three homogenizations. We see that band projection gives a better approximation. We also see that it is more efficient to truncate  $H$  than to truncate  $\bar{L}$ .

Next, the coefficient in the differential equation is changed to

$$g(x) = \begin{cases} 1/6, & 0.45 < x < 0.55, \\ 1, & \text{otherwise.} \end{cases} \quad (148)$$

All other characteristics are kept. The result is given in Fig. 3 and it shows that the relative merits of the different methods are more or less the same. The structures of the untruncated  $\bar{L}$  and  $H$  matrices are shown in Fig. 4. It should be noted that the local inhomogeneity of the full operator has spread out over a larger area, but it is still essentially local.

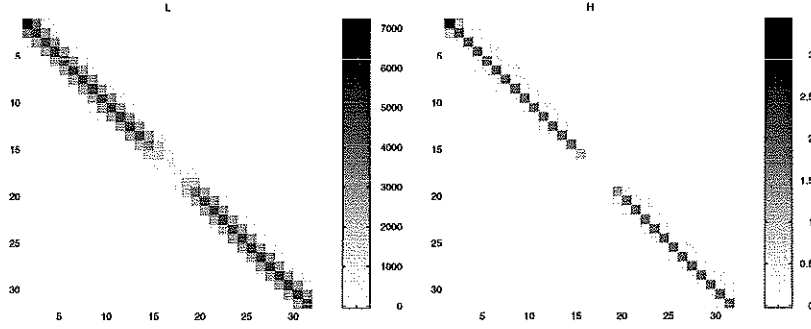


**Fig. 4.** Structure of the untruncated homogenized operators  $\bar{L}$  (left) and  $H$  (right) for the elliptic model problem,  $g(x)$  a slit. Gray level indicates absolute value of elements

### The 1D Helmholtz Equation

The equation (144) is discretized in one dimension, with the boundary conditions  $u(0) = 1$  and  $u'(1) = 0$ ,

$$\begin{aligned} -\frac{1}{h^2} \Delta_+ g_i \Delta_- u_i - \omega^2 u_i &= 0, \quad i = 1, \dots, n, \\ u_0 &= 2u(0) - u_1, \\ u_{n+1} &= u_n. \end{aligned} \quad (149)$$

We use  $\omega = 2\pi$  and the same  $g(x)$  as in (148) and again we take  $n = 256$  and use three homogenizations. We get

$$\bar{L}u = (\bar{L} - \omega^2 I)u = 0. \quad (150)$$

Truncation is performed on  $\tilde{L}$  (or  $\tilde{H}$ ) and not on  $\bar{L}$ . The result is in Fig. 5. We see that Helmholtz equation gives results similar to those of the model equation. Again band projection is more efficient than truncation and approximating  $H_j$  is more efficient than approximating  $\bar{L}$ .

### The 2D Helmholtz Equation

We consider the two-dimensional version of (144), with periodic boundary conditions in the  $y$ -direction, and at the left and right boundaries,  $u(0, y) = 1$ ,  $u_x(1, y) = 0$  respectively. This is a simple model of a plane time-harmonic wave of amplitude one entering the computational domain from the left and flowing out at the right. The discretization that we use is

$$\begin{aligned} -\frac{1}{h^2} \Delta_+^x g_{i\ell} \Delta_-^x u_{i\ell} - \frac{1}{h^2} \Delta_+^y g_{i\ell} \Delta_-^y u_{i\ell} - \omega^2 u_{i\ell} &= 0, \quad i, \ell = 1, \dots, n, \\ u_{i,0} &= u_{i,n}, \quad u_{i,n+1} = u_{i,1}, \quad u_{n+1,\ell} = u_{n,\ell} \quad u_{0,\ell} = 2 - u_{1,\ell}. \end{aligned} \quad (151)$$

This leads to the matrix equation

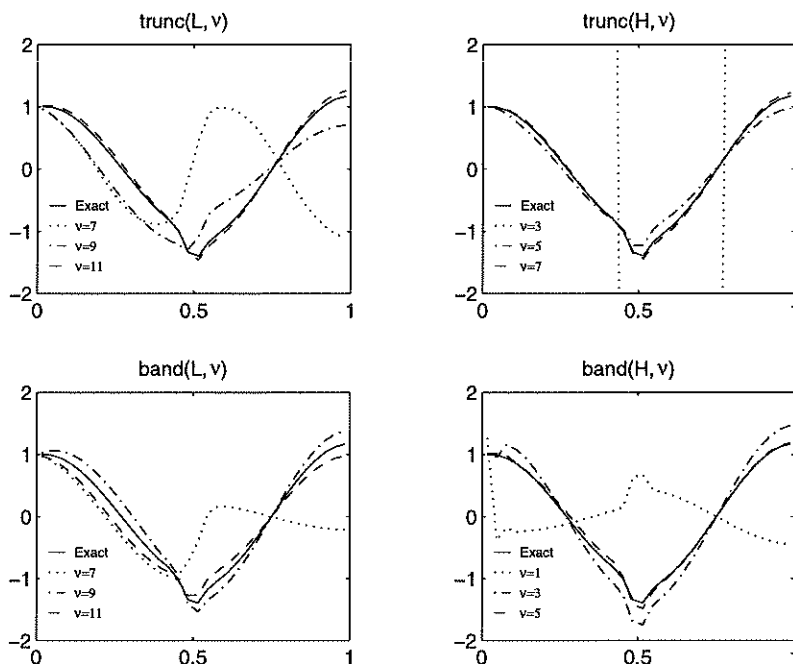
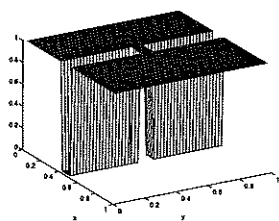


Fig. 5. Result for the Helmholtz equation,  $g(x)$  a slit, when the homogenized operator is approximated in different ways. The “exact” solution refers to the solution with the full  $32 \times 32$  homogenized operator



$$g(x, y) = \begin{cases} 10^{-4}, & 0.4 < x < 0.5 \text{ and} \\ & |y - 0.5| > 0.05, \\ 1, & \text{otherwise.} \end{cases}$$

Fig. 6. The variable coefficient  $g(x, y)$  used in the 2D Helmholtz example

$$L_{j+1}U = F, \quad U, F \in \mathbf{V}_{j+1}, \quad n = m2^{j+1}, \quad (152)$$

where  $m$  is a positive integer.  $L_{j+1}$  is homogenized following the theory for two-dimensional problems in Sect. 3.2.

As an example we choose the  $g(x, y)$  shown in Fig. 6, which models a wall with a small slit where the incoming wave can pass through. With  $\omega = 3\pi$  and  $n = 48$ , we obtained the results presented in Fig. 7.

The operator after one homogenization step is truncated according to (142). We show the results of truncation in Fig. 8, for various values of  $\nu$ . The case  $\nu = 9$  corresponds to a compression to approximately 7% of the original size. The structure of this operator is shown in Fig. 9.

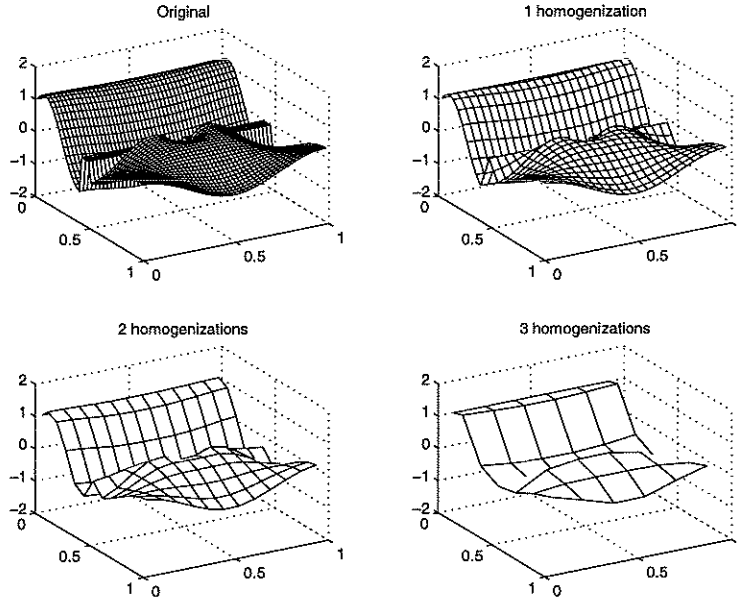


Fig. 7. Result for the 2D Helmholtz example. Solution shown for 0, . . . , 3 homogenization steps

## 4.2 Hyperbolic Problems

In this section we consider the time-dependent hyperbolic model equation in one space dimension,

$$\frac{\partial u}{\partial t} + g(x) \frac{\partial u}{\partial x} = f(x, t), \quad u(0, t) = 0, \quad u(x, 0) = b(x). \quad (153)$$

The variable coefficient  $g(x)$  is positive and bounded.

We will use three different methods to homogenize (153). First, we consider a semi-discrete form of the problem, and only homogenize the spatial part of the operator. Second, we make a correction for the extra errors introduced when neglecting the time-derivative. Third, we homogenize the full two-dimensional operator.

The most straightforward way to homogenize (153) is by a semi-discrete approximation,

$$\frac{\partial u_i}{\partial t} + \frac{1}{h} g_i \Delta_- u_i = f_i(t), \quad i = 1, \dots, n, \quad u_0 = -u_1, \quad u_i(0) = b_i, \quad (154)$$

with  $g_i = g((i - 1/2)h)$ . In matrix form we will have

$$U_t + L_{j+1} U = F, \quad 2^{j+1} = n, \quad (155)$$

which can be expressed in a wavelet basis as

$$\frac{\partial}{\partial t} \begin{pmatrix} U_f \\ U_c \end{pmatrix} + \begin{pmatrix} A_j & B_j \\ C_j & D_j \end{pmatrix} \begin{pmatrix} U_f \\ U_c \end{pmatrix} = \begin{pmatrix} F_f \\ F_c \end{pmatrix}, \quad U_f, F_f \in W_j, \quad U_c, F_c \in V_j. \quad (156)$$

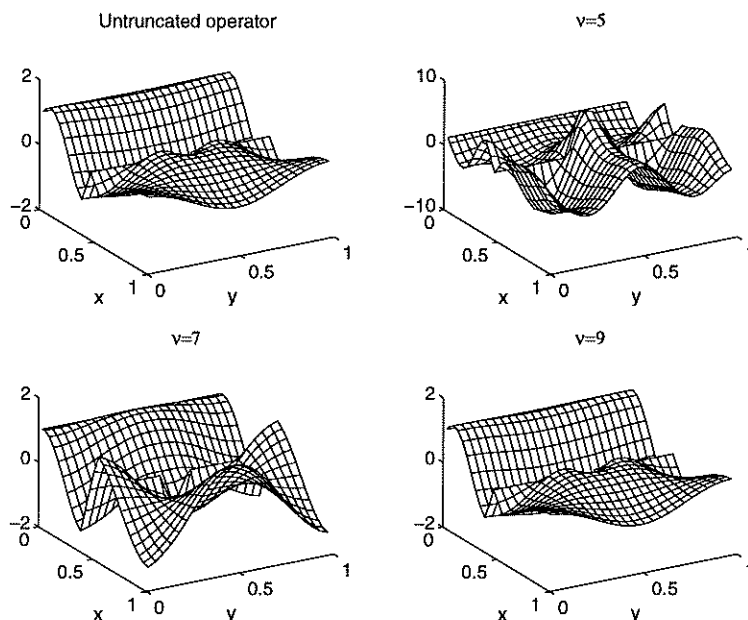


Fig. 8. Results for the 2D Helmholtz example, using the one step homogenized operator, truncated with different  $\nu$

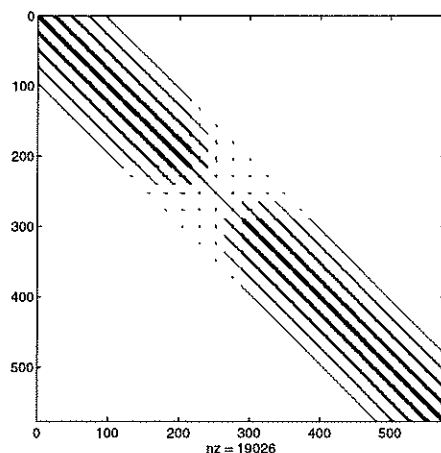


Fig. 9. Structure of the homogenized operator  $\bar{L}$ , after one homogenization step, for the 2D Helmholtz example. Elements larger than 0.1% of max value shown

In principle,  $L_{j+1}$  could be homogenized in the same way as in the elliptic case, using the Schur complement. The motivation for this is (9), which shows that when the scales of  $g(x/\varepsilon)$  become very small,  $\varepsilon \rightarrow 0$ , the effect of the time-derivative vanishes,  $\frac{\partial}{\partial t} U_f \rightarrow 0$ . As a limiting process in classical homogenization, this is fully

justified, compare [5]. This argument implies that in the first set of equations of (156),

$$\frac{\partial U_f}{\partial t} + A_j U_f + B_j U_c = F_f \Rightarrow U_f = A_j^{-1}(-B_j U_c + F_f - \frac{\partial U_f}{\partial t}), \quad (157)$$

the last term,  $-A_j^{-1} \frac{\partial}{\partial t} U_f$  is eliminated. Substitution into the second set of equations of (156) yields

$$\frac{\partial U_c}{\partial t} + \bar{L}_j U_c = \bar{F}_j, \quad (158)$$

with  $\bar{L}_j$  and  $\bar{F}_j$  defined by (104).

We found experimentally that using an approximation of the term  $-A_j^{-1} \frac{\partial}{\partial t} U_f$  improved the homogenized operator. The correction is derived by taking the time-derivative of (157),

$$\frac{\partial U_f}{\partial t} = A_j^{-1} \left( -B_j \frac{\partial U_c}{\partial t} + \frac{\partial F_f}{\partial t} - \frac{\partial^2 U_f}{\partial t^2} \right). \quad (159)$$

After a transient mode we have for the model problem (153) with  $g = \bar{g}(x/\varepsilon)$  and  $\bar{g}(y)$  1-periodic,

$$u(x, t) = \bar{u}(x, t) + \varepsilon u_1(x, x/\varepsilon, t) + \mathcal{O}(\varepsilon^2), \quad (160)$$

compare [5]. Hence,  $\frac{\partial^2}{\partial t^2} U_f$  is of the same order as  $\frac{\partial}{\partial t} U_f$  since the oscillations on the  $\varepsilon$ -scale are not functions of time and it is reasonable to neglect  $-A_j^{-1} \frac{\partial^2}{\partial t^2} U_f$  in (159) instead of  $-A_j^{-1} \frac{\partial}{\partial t} U_f$  in (157). Substituting (159) after elimination, into (156) gives

$$K_j \frac{\partial U_c}{\partial t} + (D_j - C_j A_j^{-1} B_j) U_c = F_c - C_j A_j^{-1} F_f + C_j A_j^{-2} \frac{\partial F_f}{\partial t}, \quad (161)$$

with the correction matrix

$$K_j = I + C_j A_j^{-2} B_j. \quad (162)$$

Hence, the corrected homogenized operator  $\tilde{L}_j$  and right hand side  $\tilde{F}_j$  are

$$\tilde{L}_j = K_j^{-1} \bar{L}_j, \quad \tilde{F}_j = K_j^{-1} \bar{F}_j + K_j^{-1} C_j A_j^{-2} \frac{\partial F_f}{\partial t} \quad (163)$$

and we will solve (158), with  $\tilde{L}_j, \tilde{F}_j$  substituted for  $\bar{L}_j, \bar{F}_j$  respectively.

In principle, better approximations could be obtained by reiterating the steps above. After repeated differentiations of (159) we could choose to eliminate terms involving successively higher order time derivatives of  $U_f$ . However, the condition numbers of the correction matrices produced in this manner rapidly deteriorate.

Let  $n = 128$ ,  $f \equiv 0$  and

$$b(x) = \begin{cases} \sin^2(4\pi x), & 0 \leq x \leq 0.25 \\ 0, & 0.25 < x \leq 1. \end{cases} \quad (164)$$

The result at time  $t = 1$ , is given in Fig. 10 for the case of  $g(x)$  uniformly random distributed in  $[0.1, 2]$  and  $g(x)$  as in (148). The effect of the correction is shown to the right. In these calculations, the time-integration was replaced by a fourth-order Runge-Kutta method.

Because of causality the full operator must be lower triangular in the hyperbolic case. The homogenized operator will keep this property in the Haar case. After two

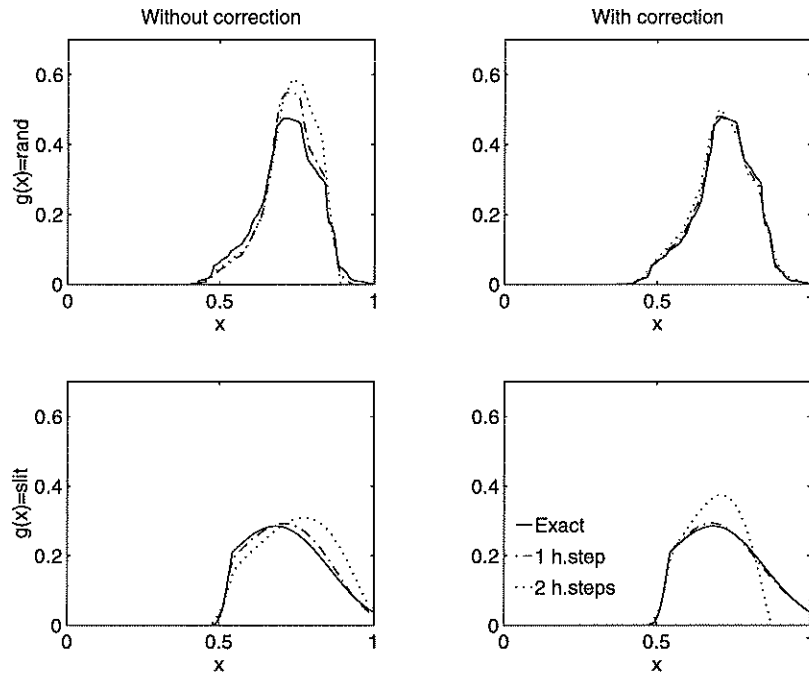


**Fig. 10.** The solution  $u(x)$  at  $t = 1$  for the hyperbolic case, using different  $g(x)$ , with and without first order correction. Solutions shown are the exact solution, computed with the full operator, and solutions computed with the operator homogenized one and two steps

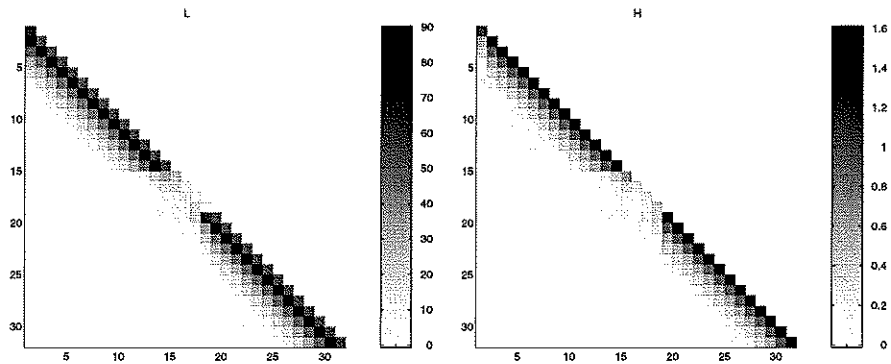


**Fig. 11.** Structure of the untruncated homogenized operators  $\bar{L}$  (left) and  $H$  (right) for the hyperbolic problem,  $g(x)$  a slit. Gray level indicates absolute value of elements



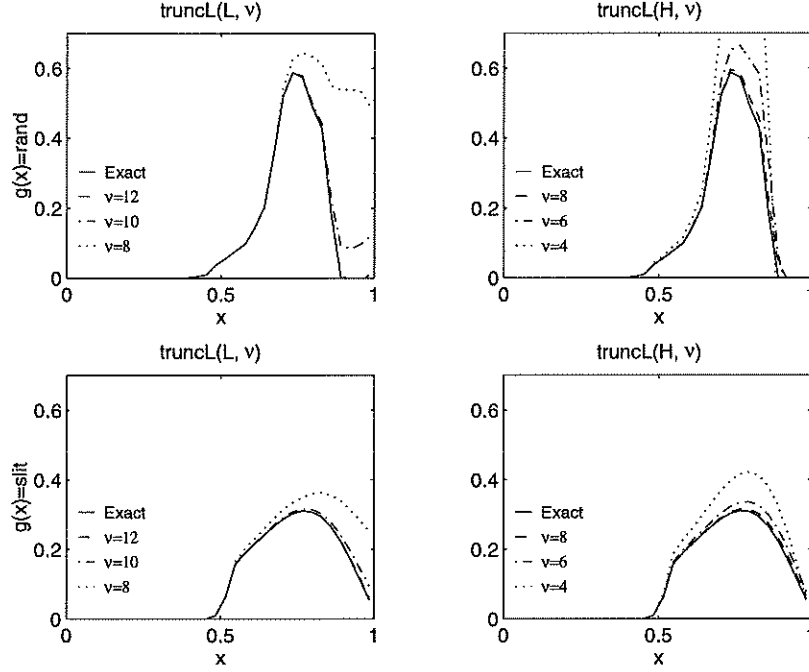


Fig. 12. Solution  $u(x)$  for the hyperbolic case, using different  $g(x)$  and different approximations of the homogenized operator. The “exact” solution refers to the solution with the full  $32 \times 32$  homogenized operator

homogenization steps the operator, with  $g(x)$  a slit, has the structure shown in Fig. 11. In view of this we approximate  $\bar{L}$  and  $H$ , see (117), by truncation to lower triangular form. In Fig. 12 results using this truncation is displayed. The same two types of  $g_\varepsilon$  as in Fig. 10 were used. Like in the elliptic case, truncating the  $H$  matrix is more efficient than truncating  $\bar{L}$ . When the correction method is used it is harder to approximate the resulting homogenized operator,  $\bar{L}$ , with a sparse matrix. It will not be as diagonal dominant as in the non-corrected case.

In our third approach we leave the semi-discrete form and instead make a full two-dimensional discretization of (153) in  $(x, t)$  space, using the implicit Euler approximation in time,

$$\begin{aligned} \frac{1}{h} \Delta_-^t u_{i\ell} + \frac{1}{h} g_i \Delta_-^x u_{i\ell} &= f_i, \quad i, \ell = 1, \dots, n, \\ u_{0,\ell} &= -u_{1,\ell}, \\ u_{i,0} &= 2b_i - u_{i,1}. \end{aligned} \tag{165}$$

Like in the two-dimensional Helmholtz case, Sect. 4.1, we arrive at a linear system of equations,

$$L_{j+1} U = F, \quad U, F \in \mathbf{V}_{j+1}, \quad n = 2^{j+1}, \tag{166}$$

which is homogenized in the standard way, with the Schur complement.

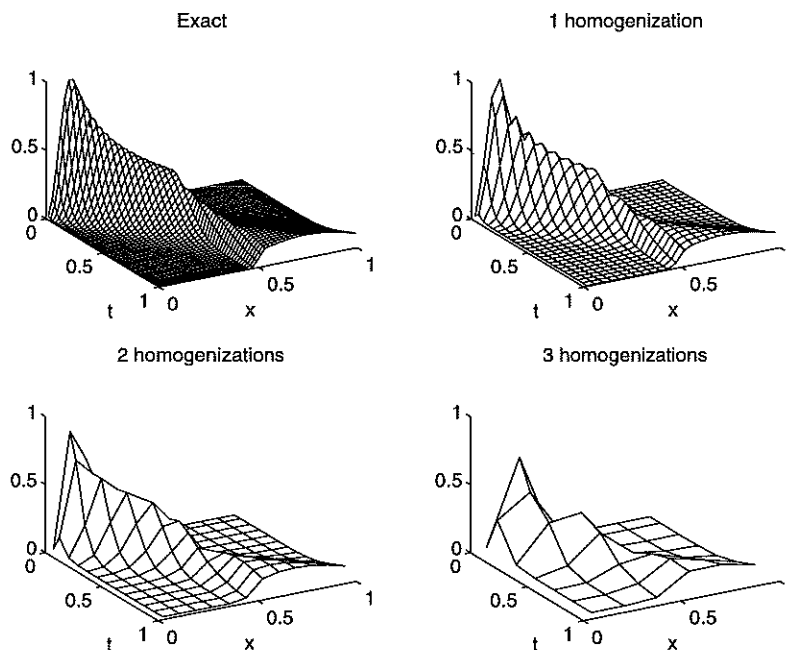


Fig. 13. Result for the 2D hyperbolic case, with  $g(x)$  a slit

Using the same data as in the semi-discrete case, but with  $n = 48$ , we get for the case of  $g$  as in (148) the results in Fig. 13. We used the untruncated homogenized operator, but its structure indicates that, like in the 2D Helmholtz case, good sparse approximations can be found.

## 5 Waveguide

In this chapter we study a waveguide filter containing a fine scale structure, to illustrate some ways of using the numerically homogenized operator  $\bar{L}$  in an application. The filter is shown in Fig. 14. It is composed of a straight waveguide with small gratings engraved on one of its sides at regular intervals. At one point the distance between two of the grating teeth is increased by 50%. This *quarter-wave step* gives a narrow-band filter effect and causes waves of one resonant frequency to pass through, while reflecting adjacent frequencies. The most important feature of the waveguide filter is the interplay between a small scale periodic structure (the gratings) and a localized inhomogeneity (the quarter-wave step). For this case, analytical homogenization techniques do not apply. The ability to separate frequencies makes the filter a useful component in many communication applications. For instance, it allows an optical communication link to be partitioned into many channels where signals can be selectively transmitted and detected. Applications can be found in [31] and [23]. The parameters used in the design of the filter determine many of its relevant properties, and it is of interest to simulate the filter numerically in order to anticipate the influence of these parameters.

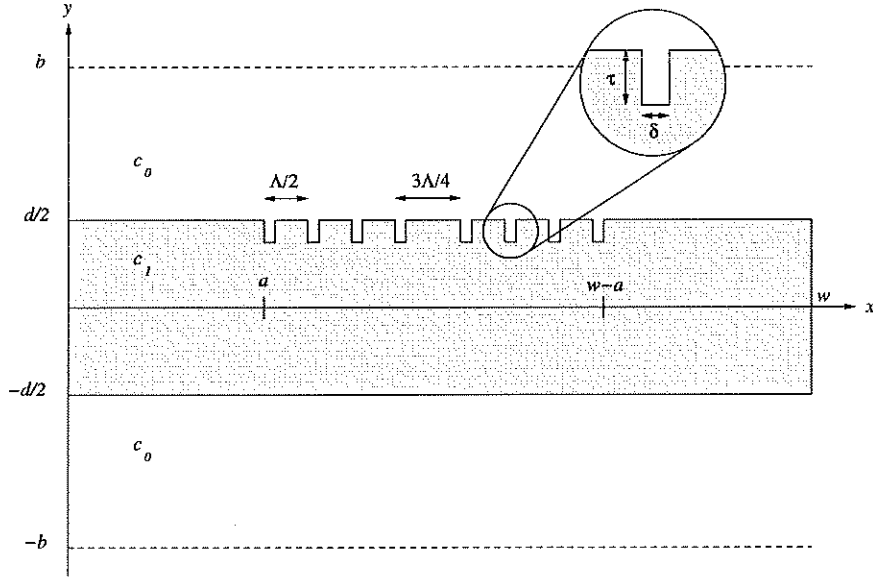


Fig. 14. Schematic picture of the waveguide with parameter specifications

We model the waveguide with the two-dimensional Helmholtz equation,

$$\nabla \cdot (c(x, y)^2 \nabla u) + \omega^2 u = 0, \quad (167)$$

where  $c(x, y)$  represents the material dependent speed of propagation. In our case,  $c$  is piecewise constant and (167) should be interpreted in the distributional sense. See [36] for more details. In Fig. 14 we specify the parameters that define the waveguide ( $w, a, d, \Lambda, \delta$  and  $\tau$ ). Related to these is  $S$ , denoting the number of gratings, which for a real filter would be a very large number. Further parameters are  $c_0$  and  $c_1$ , the propagation speeds inside and outside the waveguide, which we fix to be  $c_0 = 1$  (vacuum) and  $c_1 = 1/3.3$  (GaAs).

### 5.1 Numerical Approximation

We approximate (167) in the rectangle  $[0, w] \times [-b, b]$  on a uniform  $N \times M$  size grid. With the same notation as in Chap. 4, we use a second order scheme given by

$$\frac{1}{h^2} \Delta_+^x c_{k-1/2, \ell}^2 \Delta_-^x u_{k\ell} + \frac{1}{h^2} \Delta_+^y c_{k, \ell-1/2}^2 \Delta_-^y u_{k\ell} + \omega^2 u_{k\ell} = 0 \quad (168)$$

for  $k = 1, \dots, N$  and  $\ell = 1, \dots, M$ . This discretization corresponds to the same divergence form as the continuous problem (167), which ensures that the numerical solution satisfies the same interface conditions as the weak solution of (167) when  $c$  is discontinuous.

To complete the continuous and the discrete problems, (167, 168), extra conditions must be given at the boundary of the domain  $[0, w] \times [-b, b]$ . At  $y = \pm b$

we use a Neumann boundary condition  $u_y = 0$ , discretized with the second order approximation

$$\frac{1}{h} \Delta_+^y u_{k,0} = 0, \quad \frac{1}{h} \Delta_+^y u_{k,M} = 0, \quad k = 1, \dots, N. \quad (169)$$

This is motivated by the fact that the solution should be almost constant zero far away from the waveguide. For the boundaries at  $x = 0$  and  $x = w$  we need absorbing boundary conditions, since we are looking for a wave solution propagating along the  $x$ -axis. We use

$$\frac{1}{h} \Delta_+ u_{0,\ell} + a_1 u_{0,\ell} = a_2 u_{\text{in}}(y_\ell), \quad \frac{1}{h} \Delta_+ u_{N,\ell} + a_3 u_{N,\ell} = 0, \quad (170)$$

for  $\ell = 1, \dots, M$  with  $a_j$ ,  $j = 1, 2, 3$  chosen such that the a discrete solution of the waveguide problem without gratings satisfy both (168) and (170) exactly. Here  $u_{\text{in}}(y)$  is the wave we send into the waveguide at  $x = 0$ .

The resulting linear system of equations is then of the form

$$LU = F, \quad U, F \in V_n \otimes V_m, \quad \mathcal{L}(V_n \otimes V_m, V_n \otimes V_m), \quad (171)$$

where  $M = 2^m$  and  $N = 2^n$ .

## 5.2 Direct Simulation

As an example of how the filter works, we simulate a test problem with the specifications

$$\begin{aligned} w = 1, \quad a = 1/4, \quad S = 32, \quad d = 17/1024, \quad b = 4/128, \\ \Lambda = 32/1024, \quad \tau = 4/1024, \quad \delta = 4/1024, \quad M = 64, \quad N = 1024. \end{aligned} \quad (172)$$

The left part of Fig. 15 shows examples of solutions in the case of total reflection,  $\omega/2\pi = 44.5$ , and total transmission,  $\omega/2\pi = 45.155$ . In the right part of Fig. 15 the *frequency response* of the same filter is shown. This function measures how much power is transmitted through the filter at each frequency. For a fixed frequency the response is defined and computed as

$$T_{\text{pow}} \equiv \frac{\int_{-\infty}^{\infty} |u(w, y)|^2 dy}{\int_{-\infty}^{\infty} |u_{\text{in}}(y)|^2 dy} \approx \frac{\sum_{\ell=1}^M |u_{N,\ell}|^2}{\sum_{\ell=1}^M |u_{\text{in}}(y_\ell)|^2}. \quad (173)$$

We note that within its operational range, the filter indeed just lets through waves in a narrow frequency band. The right figure also shows the stability of the response under perturbation of the parameters  $a$  and  $b$ . The case (i) is the original test problem (172). In (ii) we modified  $a$  to  $1/8$  (and  $N = 768$ ,  $w = 3/4$ ). In (iii) we changed  $b$  to  $24/1024$  (and  $M = 48$ ). As can be seen, these perturbations only have a small effect on the response.

## 5.3 One-Dimensional Models

To reduce the complexity of solving the full Helmholtz equation (167), and to gain better understanding of the physical processes, one often wants to derive lower-dimensional models that capture the significant features of the full model. A typical model would be of the form

$$\frac{d}{dx} c_{\text{eff}}(x, \omega)^2 \frac{du_e}{dx} + \omega^2 u_e = 0, \quad (174)$$

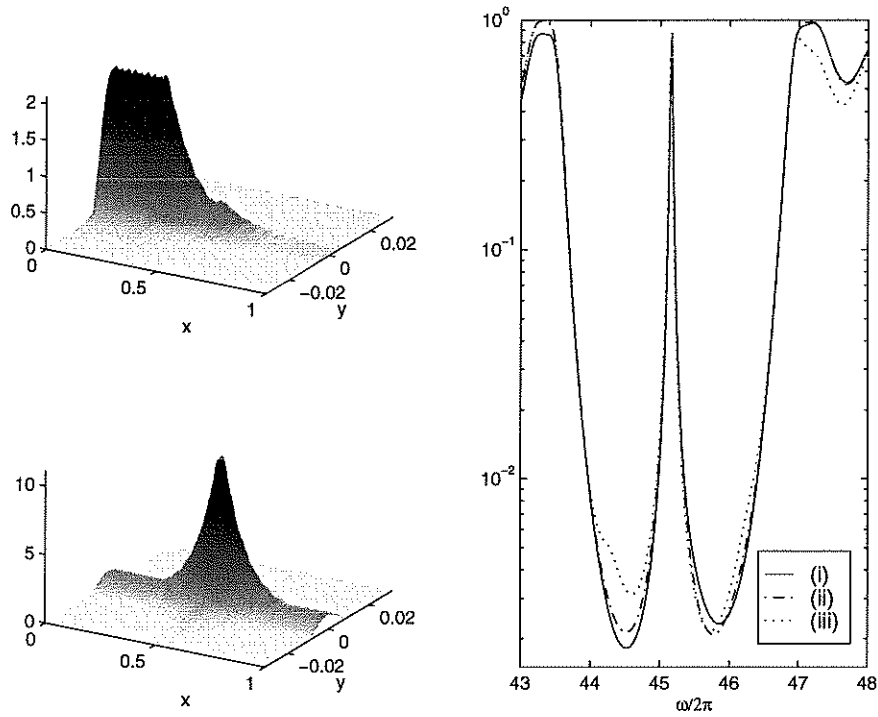


**Fig. 15.** Plots of solutions to test problem (172). Left figures show  $|u|$  for frequencies in the stopband (top left) and at resonance (bottom left). Right figure shows the frequency response  $T_{\text{pow}}(\omega)$  for the same test problem (i) and for problems with perturbed  $a$  (ii) and  $b$  (iii)

where  $u_e$  is related to  $u$ , the solution of (167), in a simple way, see e.g. [4,37]. We will here show how the homogenization technique described in Chap. 3 can be used to derive a family of one-dimensional models with different properties. In these one-dimensional models  $u_e$  is an approximation of the solution, projected in the  $y$ -direction on a space of low dimension.

The full two-dimensional operator is first homogenized multiple levels, but only in the  $y$ -direction. We hence use  $X_0 = V_n \otimes V_{n'}$  with  $m' < m$  as the small space. The operator is subsequently truncated and identified with a discretization of a one-dimensional differential operator acting on  $V_n \times \cdots \times V_n$  ( $2^{m'}$  factors). The resulting operator and right hand side approximate a system of one-dimensional partial differential equations of size  $M' = 2^{m'}$ , the number of grid points left in the  $y$ -direction. The order of the differential operator corresponds to the bandwidth of the truncated operator. In conclusion, three different parameters can be varied:

1. The size  $M'$  of the system of equations,
2. The order  $r$  of the differential operator,
3. The wavelet system used in the homogenization.

In general there is a trade-off between  $M'$  and  $r$ , such that a smaller  $M'$  requires a larger  $r$ . The reason is that the bandwidth after truncation usually needs to increase with the number of levels that an operator is homogenized in order to maintain good accuracy.

To exemplify the process described above, we derive a one-dimensional model for the test problem given by

$$\begin{aligned} w = 1, \quad a = 3/16, S = 10, \quad d = 5/64, b = 1/8, \\ \Lambda = 1/8, \tau = 1/64, \delta = 1/64, M = 16, N = 64. \end{aligned} \quad (175)$$

We use a medium size model, with  $M' = 4$ ,  $r = 2$ , and  $X_0$  given by the Daubechies wavelet system with four vanishing moments. Numerical experiments with different wavelet systems suggest that in general the higher order of the wavelets, the better the result.

Let us introduce the continuous  $4 \times 4$  system model with the unknowns  $u = (u_1, u_2, u_3, u_4)^* \in \mathbb{C}^4$ ,

$$\partial_x(B(x)\partial_x u) + C(x)u + \omega^2 u = 0, \quad B(x), C(x) : \mathbb{R} \mapsto \mathbb{R}^{4 \times 4}. \quad (176)$$

This ansatz differs from (174) in that it also has a variable coefficient in the lower order term. On the other hand, none of the coefficients are assumed to be frequency dependent. This is preferable here, since it will reduce the cost of computing the frequency response of the filter.

We now proceed as follows. The discrete two-dimensional problem is homogenized two levels in the  $y$ -direction and afterwards the unknowns in the equation  $\bar{L}\bar{u} = \bar{f}$  are reordered to the blocked form

$$\begin{pmatrix} \bar{L}_{11} & \bar{L}_{12} & \bar{L}_{13} & \bar{L}_{14} \\ \bar{L}_{21} & \bar{L}_{22} & \bar{L}_{23} & \bar{L}_{24} \\ \bar{L}_{31} & \bar{L}_{32} & \bar{L}_{33} & \bar{L}_{34} \\ \bar{L}_{41} & \bar{L}_{42} & \bar{L}_{43} & \bar{L}_{44} \end{pmatrix} \begin{pmatrix} \bar{u}_1 \\ \bar{u}_2 \\ \bar{u}_3 \\ \bar{u}_4 \end{pmatrix} = \begin{pmatrix} \bar{f}_1 \\ \bar{f}_2 \\ \bar{f}_3 \\ \bar{f}_4 \end{pmatrix}, \quad \bar{u}_i, \bar{f}_i \in V_n, \quad \bar{L}_{ij} \in \mathcal{L}(V_n, V_n). \quad (177)$$

Each of the suboperators  $\bar{L}_{ij}$  is truncated to tridiagonal form, which essentially corresponds to truncating the full operator  $\bar{L}$  to 15-diagonal form (before reordering). We identify the unknowns  $\bar{u}_i$  and  $\bar{f}_i$  with one-dimensional grid functions,  $\bar{u}_i = \{\bar{u}_{i,k}\} \approx \{u_i(x_k)\}$  and  $\bar{f}_i = \{\bar{f}_{i,k}\} \approx \{f_i(x_k)\}$  for some  $u_i$  and  $f_i$ . Furthermore, the truncated operators  $\bar{L}_{ij}$  are identified with the discretization

$$\frac{1}{h^2} \bar{L}_{ij} = \frac{1}{h^2} \Delta_+ b_{ij}(x_{k-1/2}) \Delta_- + \bar{c}_{ij}(x_k) + \frac{1}{2} \gamma_{ij}(x_k) (\mathcal{E} + \mathcal{E}^{-1}) + \omega^2 \quad (178)$$

where  $\mathcal{E}$  is the displacement operator defined by  $\mathcal{E}x_k = x_{k+1}$ . The  $\gamma_{ij}$  terms are needed since  $\bar{L}_{ij}$  is in general not symmetric. Each  $\bar{L}_{ij}$  can be seen as a discretization of a second order differential operator acting on the grid function  $\bar{u}_i$ . After assembling the suboperators by setting  $B = \{b_{ij}\}$ ,  $\bar{C} = \{\bar{c}_{ij}\}$  and  $\Gamma = \{\gamma_{ij}\}$  we get

$$\frac{1}{h^2} \Delta_+ B(x_{k-1/2}) \Delta_- U_k + \bar{C}(x_k) U_k + \frac{1}{2} \Gamma(x_k) (U_{k-1} + U_{k+1}) + \omega^2 U_k = F_k, \quad (179)$$

where we also assembled the grid functions  $U = \{\bar{u}_i\}$  and  $F = \{\bar{f}_i\}$ . If  $C(x_k) = \bar{C}(x_k) + \Gamma(x_k)$  and  $B(x_k)$  were real and independent of  $\omega$  and if  $F = 0$  this could be identified with a second order discretization of (176). Thus, the matrices  $B(x)$

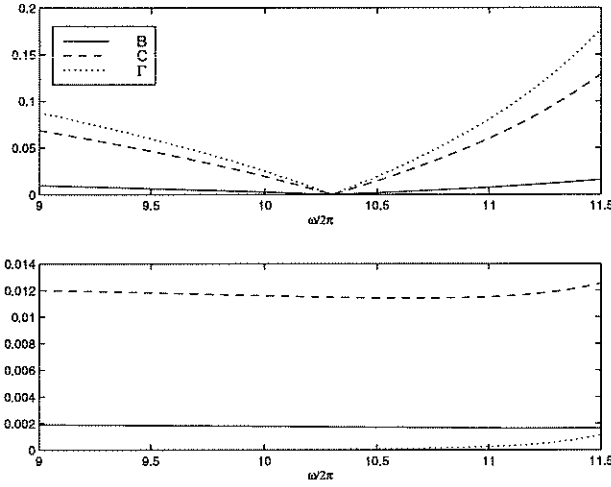


**Fig. 16.** Frequency dependency of coefficients. Relative  $L^2$ -difference between coefficients computed at  $\omega$  and at  $\omega/2\pi = 10.3$  (above). Relative  $L^2$ -difference between imaginary and real part of coefficients (below)

and  $C(x)$  represent the effective material of the waveguide, similar to  $c_{\text{eff}}(x, \omega)$  in (174).

In fact, the computed coefficients satisfy these conditions to a fairly good level of approximation, which is illustrated in Fig. 16. The coefficients are computed for a range of  $\omega$  and the relative  $L^2$ -difference, compared to the coefficients computed at resonance,  $\omega/2\pi = 10.3$ , is plotted in the top picture. The  $B(x)$  coefficients vary on the order of only 1% in the interval. In the bottom picture the  $L^2$ -norm of the imaginary part of the coefficients relative to the real part is plotted, showing that it is at worst a little more than 1%. This indicates that the model (176) is justified.

In Fig. 17 we show the frequency response computed in two different ways, and compare them with the response for the two-dimensional model. The first technique is to recompute the coefficients for each new frequency. This gives a very good agreement with the response of the full model. The second technique is to compute all coefficients, once and for all, at the resonance frequency,  $\omega/2\pi = 10.3$ . Even now the model captures the true response fairly well. We could hence calculate all parameters of the model for one single frequency and the model will remain approximately valid for the whole frequency band that we are interested in.

The computational gains can be large for the method described above. Since the bandwidth of the one-dimensional model is  $M'r$ , the cost of computing the solution for  $k$  frequencies is  $CkM'^2r^2N$  flops, plus the  $k$ -independent cost of constructing the homogenized operator. At least for large  $k$ , the work of computing the solutions dominates. Comparing this with a direct method, which requires  $CkNM^3$  flops, we get a cost ratio of

$$\frac{M'^2r^2}{M^3}, \quad (180)$$

which is often small. For the test problem (175) it equals  $1/64$ .

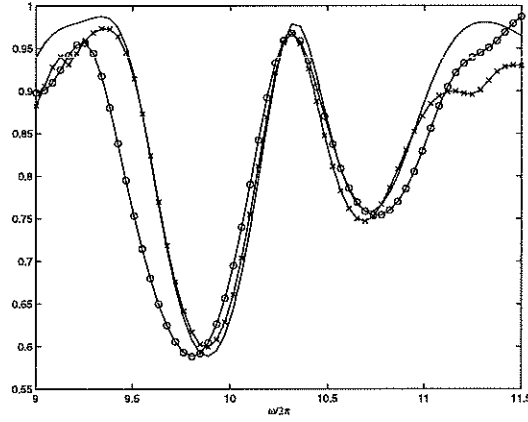


**Fig. 17.** Frequency response of test problem (175) computed using the one-dimensional model given in the text. Results shown when response was computed with the full two-dimensional model (solid line), with the one-dimensional model and coefficients recomputed for each new frequency (crosses), with the one-dimensional model and coefficients computed only once, for  $\omega/2\pi = 10.3$ , (circles)

#### 5.4 The Homogenized Operator as a Subgrid Model

In this section we will use numerical homogenization to obtain linear subgrid models of the details of the waveguide and use them to solve a large problem on a coarse grid. Our target problem is given by the parameters

$$\begin{aligned} a &= 3/16, & d &= 9/128, & b &= 1/8, & \omega/2\pi &= 11 \\ A &= 1/8, & \tau &= 3/128, & \delta &= 3/128, & M &= 32, & N &= 128, \end{aligned} \quad (181)$$

with varying length  $w$  and number of gratings  $S$ . In order to solve this problem on a coarse grid, we would need the homogenized operator  $\bar{L}$  and right hand side  $\bar{F}$ . The key observation here is that a good approximation of these can be obtained *directly from a much smaller problem*, the analogue of the cell problem in classical homogenization.

We identify four distinct parts of the waveguide: the initial part, a grating tooth, the quarter-wave step in the middle and the end part. Let  $\bar{u}^i$ ,  $\bar{u}^m$ , and  $\bar{u}^e$  denote the solution at grid points in the initial segment, middle segment and end segment. Moreover, let  $\bar{u}_k^t$  be the solution at grating tooth  $k$ . Then we can decompose  $\bar{L}\bar{u} = \bar{F}$  as

$$(\bar{L} + \delta L) \begin{pmatrix} \bar{u}^i \\ \bar{u}_1^t \\ \vdots \\ \bar{u}_{S/2}^t \\ \bar{u}^m \\ \bar{u}_{S/2+1}^t \\ \vdots \\ \bar{u}_S^t \\ \bar{u}^e \end{pmatrix} = \begin{pmatrix} \bar{F}^i \\ \bar{F}_1^t \\ \vdots \\ \bar{F}_{S/2}^t \\ \bar{F}^m \\ \bar{F}_{S/2+1}^t \\ \vdots \\ \bar{F}_S^t \\ \bar{F}^e \end{pmatrix} \quad (182)$$



where  $\bar{F}$  follows the same partitioning as  $\bar{u}$  and

$$\bar{L} = \left( \begin{array}{c} \bar{L}^i \\ \bar{L}_1^t \\ \dots \\ \bar{L}_{S/2}^t \\ \bar{L}^m \\ \bar{L}_{S/2+1}^t \\ \dots \\ \bar{L}_S^t \\ \bar{L}^e \end{array} \right) \quad (183)$$

with elements being zero outside the delineated areas. The matrix  $\delta L$  is the residual between  $\bar{L}$  and  $\tilde{L}$ , with all elements zero within the delineated areas.

With this notation we now observe that since  $\bar{L}$  is diagonal dominant,  $\delta L$  will be small. More importantly,

$$\bar{L}_k^t \approx \bar{L}_\ell^t, \quad \bar{F}_k^t \approx \bar{F}_\ell^t, \quad \forall k, \ell. \quad (184)$$

We will interpret  $\bar{L}^i$ ,  $\bar{L}^t$ ,  $\bar{L}^m$ , and  $\bar{L}^e$  together with  $\bar{F}^i$ ,  $\bar{F}^t$ ,  $\bar{F}^m$ , and  $\bar{F}^e$  as the subgrid models for the corresponding parts of the geometry. (Since  $\bar{L}_k^t$  and  $\bar{F}_k^t$  are approximately the same for all  $k$  we will henceforth drop the subindices.)

The strategy for constructing an approximation of the homogenized operator of the full problem is then clear. First, we compute an approximation of  $\bar{L}^i$ ,  $\bar{L}^t$ ,  $\bar{L}^m$ , and  $\bar{L}^e$  by homogenizing a much smaller problem. At the same time approximations of  $\bar{F}^i$ ,  $\bar{F}^t$ ,  $\bar{F}^m$ , and  $\bar{F}^e$  are also obtained. Second, we assemble the subgrid models according to the block structures of (182) and (183) to obtain an approximation of  $\bar{L}$  and  $\bar{F}$ . Finally,  $\delta L$  is neglected.

In our example we use (181) with  $w = 1$  and  $S = 10$  as our small problem. This is a well resolved problem with eight gridpoints between the gratings and approximately 15 gridpoints per effective wavelength in the  $x$ -direction. The operator is homogenized three levels in the  $y$ -direction and one level in the  $x$ -direction, corresponding to a grid size of  $M = 4$  and  $N = 64$ . This gives a very coarse resolution in the  $y$ -direction, in particular no resolution of the gratings, and a reasonable resolution in the  $x$ -direction. This grid size should be enough to represent the solution in a quantitatively correct way.

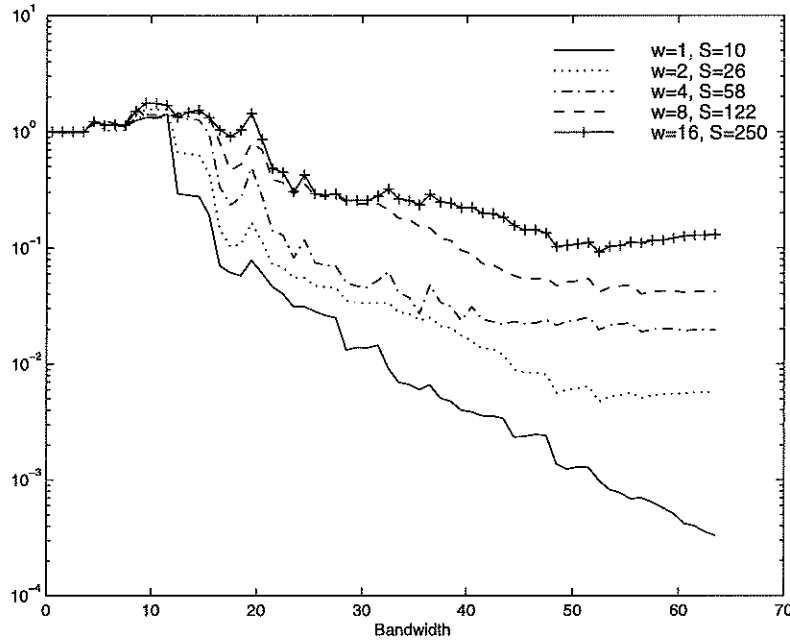


Fig. 18. Result of the subgrid technique. Relative  $L^2$ -error of solution as a function of the bandwidth

For the large problems denote the corresponding parameters with a prime sign. We will have  $w' > 1$  and  $S' > 10$  and we set  $\bar{L}^{i'} = \bar{L}^i$ ,  $\bar{L}^{m'} = \bar{L}^m$ ,  $\bar{L}^{e'} = \bar{L}^e$ , and

$$\bar{L}_k^{t'} = \begin{cases} \bar{L}_k^t & 1 \leq k \leq 2, \\ \bar{L}_3^t & 3 \leq k \leq S'/2 - 2, \\ \bar{L}_{k+(S-S')/2}^t & S'/2 - 1 \leq k \leq S'/2 + 2, \\ \bar{L}_{S/2+3}^t & S'/2 + 3 \leq k \leq S' - 2, \\ \bar{L}_{k+S-S'}^t & S' - 1 \leq k \leq S'. \end{cases} \quad (185)$$

So far we have deliberately been vague about the exact size of the areas in (183), and hence the size of the subgrid models. We now introduce a parameter  $\nu$ , the band width of  $\bar{L}$ , with which we all sizes can be defined at the same time. The value of  $\nu$  will determine the accuracy of the solution.

The results of this computation is shown in Fig. 18, where the relative  $L^2$ -error between the solution computed using the subgrid technique and the exact solution, projected onto the coarse subspace, is plotted as a function of  $\nu$ , for five different problem sizes. Our small problem,  $w = 1, S = 10$  is also included, for comparison, in which case  $\nu$  just indicates the bandwidth of the truncated operator. Even for a problem 16 times as large as the small problem, the relative  $L^2$ -error can be reduced to 10%, by choosing  $\nu$  big enough. Note that even when the relative  $L^2$ -error is rather large, a good quantitative picture of the solution is obtained in the interior of the waveguide. This is exemplified for the case of  $w = 16$  and  $\nu = 22$

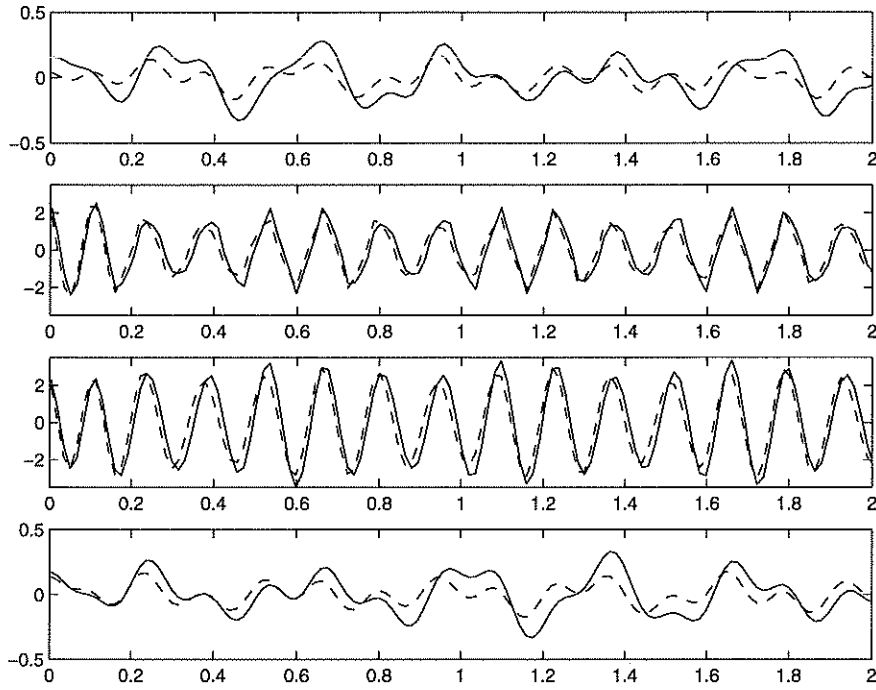


**Fig. 19.** Result of the large  $w = 16$  problem approximated with  $\nu = 22$ . Plot of exact solution (solid) and approximate solution (dashed) as a function of  $x$  for four  $y$ -values corresponding to the four grid points in the  $y$ -direction of the coarse mesh. Real part of  $u$  shown in the  $x$ -interval  $[0, 2]$ , the region with the largest errors.

in Fig. 19, where the part of the solution with the largest errors is plotted. The relative  $L^2$ -error in this case is of the order of 50%.

To estimate the gain in using the subgrid technique, let  $M$  and  $N$  denote the grid size of the large problem. The exact operator has a bandwidth of  $M$ . The cost to solve this problem is therefore  $CNM^3$  flops with a direct solver. Suppose our coarse grid is of the size  $N/2^n$  and  $M/2^m$ , corresponding to homogenization  $n$  times in the  $x$ -direction and  $m$  times in the  $y$ -direction. The direct solution using the subgrid model then costs  $CNM\nu^2/2^{n+m}$  giving a ratio between the costs of

$$2^{-n-m} \left( \frac{\nu}{M} \right)^2, \quad (186)$$

In our largest case,  $w = 16$ , with  $\nu = 45$ , we get an approximate ratio of  $1/8$ . We must also compute the subgrid model, although this only needs to be done once for all five computations above, and for a fixed grid size  $M', N'$  that can be considerably smaller than  $M, N$ . This cost is dominated by the other factors.

## 6 Multigrid

Many properties of the homogenized operator closely approximates those of the original operator. The lower eigenvalues and the corresponding eigenfunctions are, for example, well approximated in elliptic problems, see Santosa and Vogelius [40] for the classical case, and for the numerical case, Beylkin and Coult [9]. It is thus natural to try using an approximation of the homogenized operator as the coarse grid operator in a multigrid scheme. The largest potential advantage would be for problems where traditional multigrid is less efficient. Elliptic problems with highly oscillatory or strongly discontinuous coefficients are typical examples. Another class of such examples are advection dominated advection diffusion problems. For these equations the lower eigenmodes have large high derivatives and standard coarsening methods does not give satisfactory convergence. The coarser grids can not resolve the oscillations and it is therefore better to use an operator where these oscillations are not explicitly present but where there effect is taken into account.

In [19,20] this idea was explored and it was shown that using the numerical approximations of the analytically homogenized operator could be advantageous as a coarse grid operator for certain problems.

There are some factors, which make it more attractive to use the numerically homogenized operator, as developed in this paper, rather than the analytic form. A wider class of problems can be reached. Strict periodicity is not essential. Furthermore there are natural wavelet based prolongations and restrictions matching the definition of the coarse grid operator.

### 6.1 Algorithms

Let the system of linear equations,

$$L_h U_h = F_h, \quad (187)$$

come from the discretization of a differential equation, (1), on some grid  $\Omega_h$ , where  $h$  represents the step size.

For notational purposes, we briefly describe the  $V$ -cycle method used in this context. Given an interpolation operator,  $I_{2h}^h$  where the superscript refers to the fine grid and the subscript refers to the coarse grid, and a restriction operator,  $I_h^{2h}$ , we can define a multigrid method recursively. The description of the two-level method is as follows. First, relax one or a few steps on the fine grid  $\Omega_h$  to get an initial approximation  $U_h$ . Then, compute the residual  $R_h = F_h - L_h U_h$ , restrict the residual to the coarse grid  $\Omega_{2h} : R_{2h} = I_h^{2h} R_h$ , and solve the residual equation,

$$L_{2h} E_{2h} = R_{2h}, \quad (188)$$

on the coarse grid. Set  $U_h = U_h + I_{2h}^h E_{2h}$  and relax again one or a few steps on the fine grid. This describes the two-level method. Based on this, we define the  $V$ -cycle multigrid scheme recursively.

The first step in the wavelet homogenization of (187) can be written

$$\mathcal{W}L_h\mathcal{W}^*\mathcal{W}U = \begin{pmatrix} A & B \\ C & D \end{pmatrix} \begin{pmatrix} U_f \\ U_c \end{pmatrix} = \begin{pmatrix} F_f \\ F_c \end{pmatrix} = \mathcal{W}F_h. \quad (189)$$

Calculating the inverse of the factorization, and solving for  $U$ , it is natural that the interpolation and restriction operators should be defined by,

$$I_{2h}^h = \bar{P}^* - \bar{Q}^* A^{-1} B, \quad I_h^{2h} = (I_{2h}^h)^*, \quad \mathcal{W} = \begin{pmatrix} \bar{Q} \\ \bar{P} \end{pmatrix} \quad (190)$$

where, as before,  $\bar{P}^*$  and  $\bar{Q}^*$  are bases for the scaling and wavelet spaces respectively. The coarse grid operator should be

$$\bar{L}_{2h} = D - CA^{-1}B, \quad (191)$$

which is the Schur complement. Although the matrices  $A$ ,  $B$ ,  $C$  and  $D$  are as sparse as the original operator  $L_h$ ,  $A^{-1}$  is not. We observe that the fill-in that results from inversion decays exponentially as we move away from the original structure. This was discussed in Chap. 3.

The above procedure may be repeatedly applied until the desired coarseness is reached. Although the level of fill-in in the operator  $A^{-1}$  increases, the magnitude of the values decreases as we go away from the diagonal. This property of decay makes compression possible. Properties of wavelets play here an important role. In practice a compressed version  $\bar{L}_{2h}$  of  $\bar{L}_{2h}$  should be used. One thing to keep in mind is that the number of gridpoints in each coordinate direction must be an even number.

One step towards improving efficiency is to avoid computing the inverse exactly. To this end, we use  $ILU(0)$  to compute the incomplete  $LU$  factorization, and then use a sequence of forward and backward substitutions to compute the inverse. For the compression, we use a thresholding procedure. Any values that appear in the inverse in locations that hold zero values in  $D$  are set to zero, thus eliminating any fill-in over the original matrix,  $D$ . We will call this method the truncated wavelet multigrid method, and we will refer to the original method as the dense or full wavelet multigrid method.

## 6.2 Numerical Examples

We shall give a few examples in which the wavelet based multigrid method has been applied to two dimensional model problems. The examples are from De Leon, [30].

In the first set of examples the elliptic operator is,

$$L_\epsilon = -\nabla \cdot g(x, y) \nabla \quad (192)$$

for a Dirichlet problem on the unit square. The standard 5-point numerical approximation is applied to  $16 \times 16$  and  $32 \times 32$  grids, resulting in system matrices of size  $256 \times 256$  and  $1024 \times 1024$  respectively.

The coefficient  $g(x, y)$  is oscillatory and two examples are studied,

$$g(x, y) = 1 + 0.8 \sin(10\sqrt{2}\pi x), \quad (193)$$

$$g(x, y) = 1 + 0.8 \sin(10\sqrt{2}\pi(x - y)). \quad (194)$$

The analytically homogenized operators are,

$$\bar{L} = -\mu \frac{\partial^2}{\partial x^2} - \bar{a} \frac{\partial^2}{\partial y^2}, \quad (195)$$

$$\bar{L} = -\frac{\mu + \bar{a}}{2} \frac{\partial^2}{\partial x^2} + (\bar{a} - \mu) \frac{\partial^2}{\partial x \partial y} - \frac{\mu + \bar{a}}{2} \frac{\partial^2}{\partial y^2}, \quad (196)$$

respectively, with

$$\mu = \left( \int_0^1 (1 + 0.8 \sin(2\pi x))^{-1} dx \right)^{-1}, \tag{197}$$

$$\bar{a} = \int_0^1 1 + 0.8 \sin(2\pi x) dx. \tag{198}$$

Convergence results are given in Fig. 20 for the Haar case. Comparison is made with the standard finite difference multigrid, [22], and with standard finite difference multigrid with the coarse grid operator replaced by a difference approximation of  $\bar{L}$  above. The effect of compression can be seen in Fig. 21 for booth Haar and Daubechies wavelets with four vanishing moments.

Consider also a problem with piecewise constant  $g(x, y)$  in the form of a checker-board pattern with 16 squares and the  $g$ -values 1 and  $10^5$ . The standard multigrid method does not converge and we compare with an algebraic multigrid method, [38]. The wavelet technique works quite well but the convergence rate is reduced if the compression is too extreme, see Fig. 22.

Finally we approximate the advection diffusion problem,

$$-\varepsilon \Delta u + b \cdot u = 0, \quad x \in \Omega, \tag{199}$$

$$u = f(x, y), \quad x \in \partial\Omega, \tag{200}$$

where  $\Omega$  is a unit square and  $\|b\| \gg \varepsilon > 0$ . The five point formula is used for the Laplacian and upwind differencing for the advection term,

$$b(x, y) = ((2y - 1)(1 - x^2), 2xy(y - 1)). \tag{201}$$

Figure 23 shows that the convergence rate is quite good and essentially independent of the stepsize. In this case the convergence does not deteriorate with  $ILU(0)$  and compression.

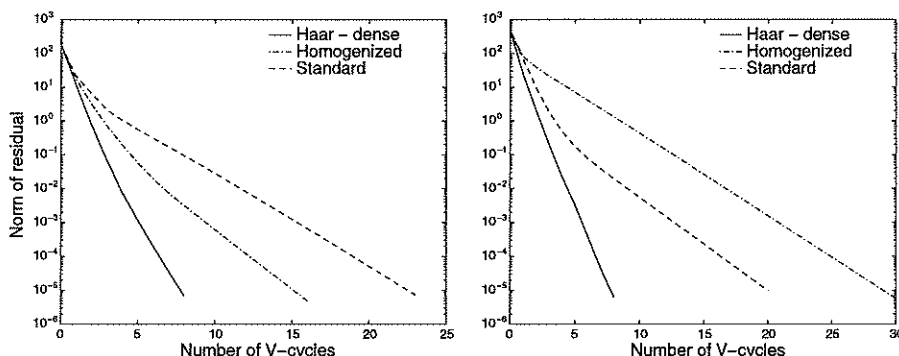


Fig. 20. Convergence result for  $g(x, y)$  defined by (193). Three level V-cycle with one Gauss-Seidel smoothing iteration is used. Left frame  $16 \times 16$  grid, right frame  $32 \times 32$  grid

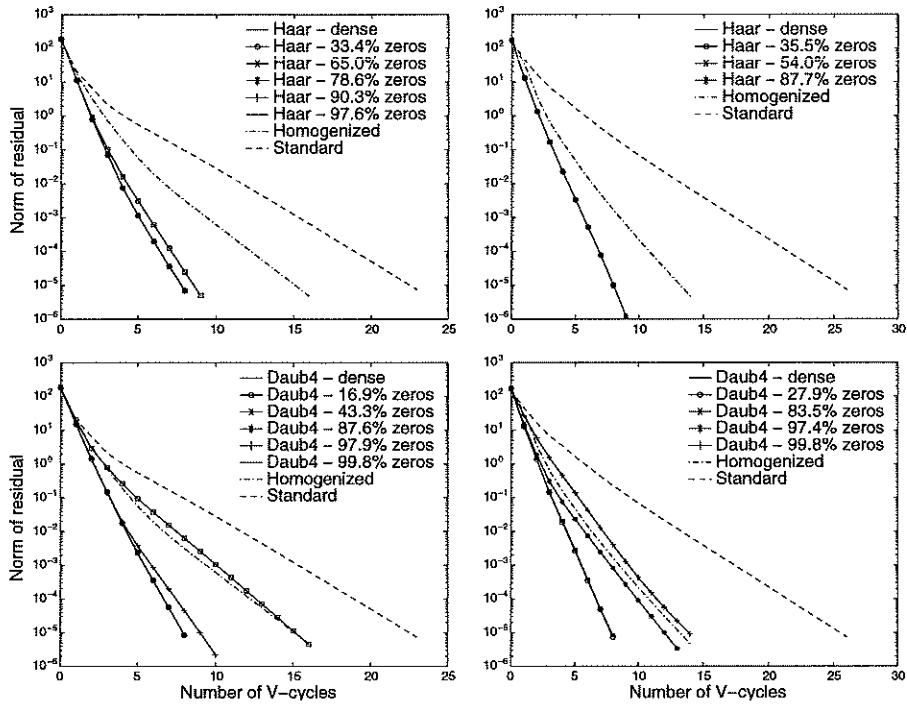


Fig. 21. Convergence result for  $g(x, y)$  defined by (193) in left frames and by (194) in right frames. Three level V-cycle with one Gauss-Seidel smoothing iteration is used. Fine grid is  $16 \times 16$ . Percentage of zeros is for coarse grid operator, second level

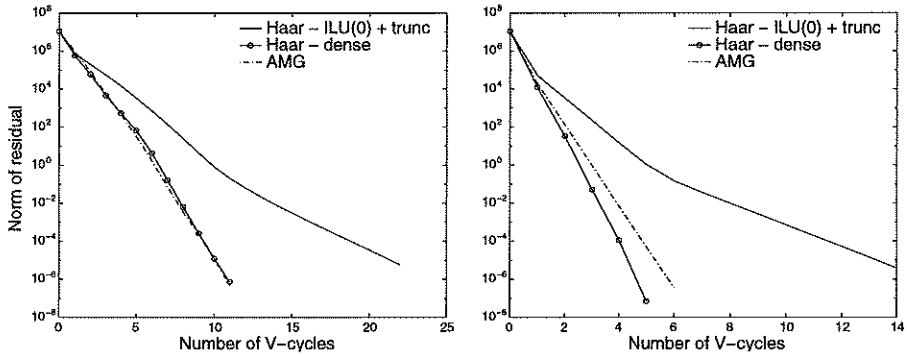
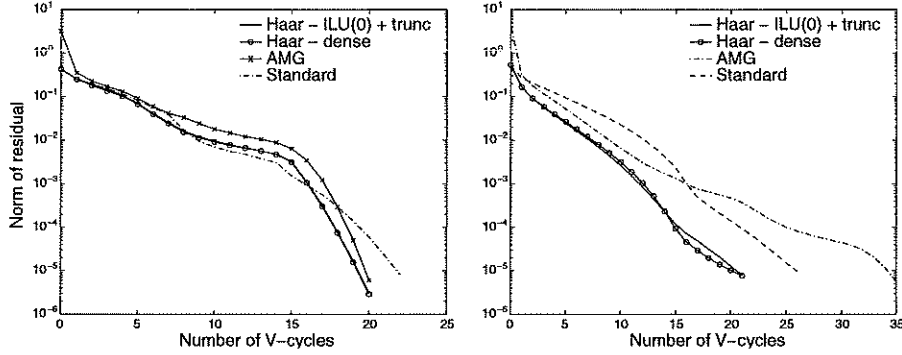


Fig. 22. Convergence result for 2-level iteration,  $g(x, y)$  from checkerboard problem on  $16 \times 16$  grid. Left frame 1 Gauss-Seidel smoothing iteration, right frame 5 Gauss-Seidel smoothing iterations



**Fig. 23.** Convergence result for advection diffusion problem. Left frame  $16 \times 16$  grid, right frame  $32 \times 32$  grid. Two level V-cycle with one Gauss-Seidel smoothing iteration is used

## 7 Nonlinear Equations

Homogenization of nonlinear equations are usually much more complicated than the linear equations we have considered so far. For some equations, however, the linear numerical homogenization methods described above generalize. The basic assumption needed is that the fine scale part of the solution is small so that we can linearize around the coarse scale. The ideas in this chapter were developed by Beylkin, Brewster and Gilbert in [7]. See also [27].

Suppose  $L_{j+1} : V_{j+1} \mapsto V_{j+1}$  is a nonlinear operator. Using the same notation as in Sect. 3.2, the nonlinear decomposition of  $L_{j+1}(U) = F$  can be written

$$\begin{aligned}
 & \mathcal{W}_j L_{j+1}(\mathcal{W}_j^* \mathcal{W}_j U) \\
 &= \left( \tilde{Q}_j \left( L_{j+1} \left( \tilde{Q}_j^* U_f + \tilde{P}_j^* U_c \right) - L_{j+1} \left( \tilde{P}_j^* U_c \right) \right) + \tilde{Q}_j L_{j+1} \left( \tilde{P}_j^* U_c \right) \right) \\
 &= \left( \tilde{P}_j \left( L_{j+1} \left( \tilde{Q}_j^* U_f + \tilde{P}_j^* U_c \right) - L_{j+1} \left( \tilde{P}_j^* U_c \right) \right) + \tilde{P}_j L_{j+1} \left( \tilde{P}_j^* U_c \right) \right) \\
 &\equiv \begin{pmatrix} A_j(U_f, U_c) + B_j(U_c) \\ C_j(U_f, U_c) + D_j(U_c) \end{pmatrix} = \mathcal{W}_j F = \begin{pmatrix} F_f \\ F_c \end{pmatrix}. \tag{202}
 \end{aligned}$$

Like in the linear case,  $U_f$  can be eliminated from the equations and the homogenized operator is

$$\bar{L}_j(U_c) = D_j(U_c) + C_j(A_j^{-1}(F_f - B_j(U_c), U_c)), \tag{203}$$

where  $A_j^{-1}(u, v)$  is the solution  $w$  to  $A_j(w, v) = u$ .

Consider nonlinear operators of the type

$$L(u) = \int_0^x G(t, u(t)) dt + H(x, u(x)), \tag{204}$$

The equation  $L(u) = f$  could result for instance from a nonlinear ODE such as

$$\frac{d}{dx} H(x, u) = -G(x, u), \quad H(0, u(0)) = f. \tag{205}$$



For simplicity we here let  $u$  be a scalar function,  $G, H \in C^\infty$  and  $f = \text{const}$ . Similar derivations can be made also for systems of equations, non-smooth coefficients and variable  $f$ . One application that was studied in [27], is the steady state equations for

$$\begin{aligned} u_t &= u_{xx} - u^3 + u - v, \\ v_t &= \delta v_{xx} + \varepsilon(u + a_1(x)v + a_0(x)), \end{aligned} \quad (206)$$

which can be formulated as a system of nonlinear ODEs. These are the Fitzhugh Nagumo equations with diffusing inhibitor, widely used as a model for pattern formation in excitable reaction-diffusion systems.

For the discretization of (204) we use the Haar basis, but since  $G$  and  $H$  are nonlinear, it is more convenient to rescale and approximate cell averages of  $u$  instead of its Haar basis coefficients. Hence, we introduce  $P_j = \bar{P}_j/\sqrt{2}$  and  $Q_j = \sqrt{2}\bar{Q}_j$ . Define the grid  $\mathbf{x}_{j+1} = \{\mathbf{x}_{j+1,k}\} = \{(k+1/2)2^{-(j+1)}\}$  and the grid function  $\mathbf{u}_{j+1} = \{u_{j+1,k}\} \approx 2^{(j+1)/2} P_{V_{j+1}} u(x)$ , where  $k = 0, \dots, 2^{j+1} - 1$  and  $P_{V_{j+1}}$  is the orthogonal projection in  $L^2([0,1])$  to the Haar scaling space  $V_{j+1}$ . Furthermore, recursively define the successively coarser grids  $\mathbf{x}_j = P_j \mathbf{x}_{j+1}$ , cell averages  $\mathbf{u}_j = \mathbf{u}_{j+1}^c = P_j \mathbf{u}_{j+1}$  and the fine scale parts  $\mathbf{u}_{j+1}^f = Q_j \mathbf{u}_{j+1}$ . We have the following discretization of  $L(u) = f$ ,

$$L_{j+1}(\mathbf{u}_{j+1}) = K_{j+1}G(\mathbf{x}_{j+1}, \mathbf{u}_{j+1}) + H(\mathbf{x}_{j+1}, \mathbf{u}_{j+1}) = f, \quad (207)$$

where

$$K_{j+1} = \delta_{j+1} \begin{pmatrix} \frac{1}{2} & 0 & \dots & 0 \\ 1 & \ddots & \ddots & \vdots \\ \vdots & \ddots & \ddots & 0 \\ 1 & \dots & 1 & \frac{1}{2} \end{pmatrix} \in \mathbb{R}^{2^{j+1} \times 2^{j+1}}, \quad \delta_{j+1} = 2^{-(j+1)}, \quad (208)$$

and  $G, H$  being applied elementwise to its vector arguments, e.g.  $G(\mathbf{x}_j, \mathbf{u}_j) = \{G(\mathbf{x}_{j,k}, u_{j,k})\}$ . The following easily verifiable formulae hold

$$Q_j K_{j+1} = -\frac{\delta_j}{2} P_j, \quad P_j K_{j+1} = K_j P_j + \frac{\delta_j}{8} Q_j. \quad (209)$$

After also rescaling  $B_j$  and  $A_j$  we get

$$B_j(\mathbf{u}_j) = -\frac{\delta_j}{2} P_j G(\mathbf{x}_{j+1}, 2P_j^* \mathbf{u}_j) + Q_j H(\mathbf{x}_{j+1}, 2P_j^* \mathbf{u}_j), \quad (210)$$

$$\begin{aligned} A_j(\mathbf{u}_{j+1}^f, \mathbf{u}_j) &= -\frac{\delta_j}{2} P_j \left( G(\mathbf{x}_{j+1}, Q_j^* \mathbf{u}_{j+1}^f / 2 + 2P_j^* \mathbf{u}_j) - G(\mathbf{x}_{j+1}, 2P_j^* \mathbf{u}_j) \right) \\ &\quad + Q_j \left( H(\mathbf{x}_{j+1}, Q_j^* \mathbf{u}_{j+1}^f / 2 + 2P_j^* \mathbf{u}_j) - H(\mathbf{x}_{j+1}, 2P_j^* \mathbf{u}_j) \right). \end{aligned} \quad (211)$$

When  $G$  and  $H$  are linear functions of  $u$ , (204) reduces to (120), and  $G(\mathbf{x}_{j+1}, \mathbf{u}_{j+1}) = \text{diag}(a(\mathbf{x}_{j+1}))\mathbf{u}_{j+1}$ ,  $H(\mathbf{x}_{j+1}, \mathbf{u}_{j+1}) = \text{diag}(b(\mathbf{x}_{j+1}))\mathbf{u}_{j+1}$ . Consequently,  $A_j$  is diagonal and the homogenization step is very easy, as was mentioned in Sect. 3.3. In the nonlinear case,  $A_j(\mathbf{u}_{j+1}^f, \mathbf{u}_j)$  is still local, and its jacobian with respect to  $\mathbf{u}_{j+1}^f$  for fixed  $\mathbf{u}_j$  is diagonal.

In order to treat the nonlinear case, we make the simplifying assumption that  $\delta_j \sim \mathbf{u}_{j+1}^f$  is small. We then have the Taylor expansions,

$$P_j G(\mathbf{x}_{j+1}, \mathbf{u}_{j+1}) = G(\mathbf{x}_j, \mathbf{u}_j) + \frac{\delta_j^2}{8} G_{xx}(\mathbf{x}_j, \mathbf{u}_j) + \frac{\delta_j \mathbf{u}_{j+1}^f}{4} G_{xu}(\mathbf{x}_j, \mathbf{u}_j) + \frac{(\mathbf{u}_{j+1}^f)^2}{8} G_{uu}(\mathbf{x}_j, \mathbf{u}_j) + \mathcal{O}(\delta_j^4), \quad (212)$$

$$Q_j G(\mathbf{x}_{j+1}, \mathbf{u}_{j+1}) = \delta_j G_x(\mathbf{x}_j, \mathbf{u}_j) + \mathbf{u}_{j+1}^f G_u(\mathbf{x}_j, \mathbf{u}_j) + \mathcal{O}(\delta_j^3), \quad (213)$$

where, again, all functions are applied elementwise. This gives the simplified expressions

$$B_j(\mathbf{u}_j) = -\frac{\delta_j}{2} G(\mathbf{x}_j, \mathbf{u}_j) + \delta_j H_x(\mathbf{x}_j, \mathbf{u}_j) + \mathcal{O}(\delta_j^3) \quad (214)$$

$$A_j(\mathbf{u}_{j+1}^f, \mathbf{u}_j) = \mathbf{u}_{j+1}^f H_u(\mathbf{x}_j, \mathbf{u}_j) + \mathcal{O}(\delta_j^3). \quad (215)$$

Hence, the solution to the cellproblem  $A_j(\mathbf{u}_{j+1}^f, \mathbf{u}_j) = -B_j(\mathbf{u}_j)$  satisfies

$$\mathbf{u}_{j+1}^f(\mathbf{x}_j, \mathbf{u}_j) = \delta_j \frac{G(\mathbf{x}_j, \mathbf{u}_j) - 2H_x(\mathbf{x}_j, \mathbf{u}_j)}{2H_u(\mathbf{x}_j, \mathbf{u}_j)} + \mathcal{O}(\delta_j^3). \quad (216)$$

We also compute approximations of  $C_j$  and  $D_j$ ,

$$\begin{aligned} D_j(\mathbf{u}_j) &= P_j K_{j+1} G(\mathbf{x}_{j+1}, 2P_j^* \mathbf{u}_j) + P_j H(\mathbf{x}_{j+1}, 2P_j^* \mathbf{u}_j) \\ &= K_j \left( G(\mathbf{x}_j, \mathbf{u}_j) + \frac{\delta_j^2}{8} G_{xx}(\mathbf{x}_j, \mathbf{u}_j) \right) + H(\mathbf{x}_j, \mathbf{u}_j) \\ &\quad + \frac{\delta_j^2}{8} H_{xx}(\mathbf{x}_j, \mathbf{u}_j) + \frac{\delta_j^2}{8} G_x(\mathbf{x}_j, \mathbf{u}_j) + \mathcal{O}(\delta_j^4), \end{aligned} \quad (217)$$

$$\begin{aligned} C_j(\mathbf{u}_{j+1}^f, \mathbf{u}_j) &= K_j P_j \left( G(\mathbf{x}_{j+1}, \mathbf{u}_{j+1}) - G(\mathbf{x}_{j+1}, 2P_j^* \mathbf{u}_j) \right) \\ &\quad + \frac{\delta_j}{8} Q_j \left( G(\mathbf{x}_{j+1}, \mathbf{u}_{j+1}) - G(\mathbf{x}_{j+1}, 2P_j^* \mathbf{u}_j) \right) \\ &\quad + P_j \left( H(\mathbf{x}_{j+1}, \mathbf{u}_{j+1}) - H(\mathbf{x}_{j+1}, 2P_j^* \mathbf{u}_j) \right) \\ &= K_j \left( \frac{\delta_j \mathbf{u}_{j+1}^f}{4} G_{xu}(\mathbf{x}_j, \mathbf{u}_j) + \frac{(\mathbf{u}_{j+1}^f)^2}{8} G_{uu}(\mathbf{x}_j, \mathbf{u}_j) \right) \\ &\quad + \frac{\delta_j \mathbf{u}_{j+1}^f}{8} G_u(\mathbf{x}_j, \mathbf{u}_j) + \frac{\delta_j \mathbf{u}_{j+1}^f}{4} H_{xu}(\mathbf{x}_j, \mathbf{u}_j) \\ &\quad + \frac{(\mathbf{u}_{j+1}^f)^2}{8} H_{uu}(\mathbf{x}_j, \mathbf{u}_j) + \mathcal{O}(\delta_j^4). \end{aligned} \quad (218)$$

Substituting (216) into the expressions for  $C_j$  and  $D_j$  gives a fourth order approximation of  $\bar{L}_j$ ,

$$\bar{L}_j(\mathbf{u}_j) = K_j \bar{G}(\mathbf{x}_j, \mathbf{u}_j) + \bar{H}(\mathbf{x}_j, \mathbf{u}_j) + \mathcal{O}(\delta_j^4), \quad (219)$$

where

$$\begin{aligned} \bar{G}(\mathbf{x}_j, \mathbf{u}_j) &= G(\mathbf{x}_j, \mathbf{u}_j) + \frac{\delta_j^2}{8} G_{xx}(\mathbf{x}_j, \mathbf{u}_j) + \frac{\delta_j \mathbf{u}_{j+1}^f}{4} G_{xu}(\mathbf{x}_j, \mathbf{u}_j) \\ &\quad + \frac{(\mathbf{u}_{j+1}^f)^2}{8} G_{uu}(\mathbf{x}_j, \mathbf{u}_j), \end{aligned} \quad (220)$$

$$\begin{aligned} \bar{H}(\mathbf{x}_j, \mathbf{u}_j) &= H(\mathbf{x}_j, \mathbf{u}_j) + \frac{\delta_j^2}{8} H_{xx}(\mathbf{x}_j, \mathbf{u}_j) + \frac{\delta_j \mathbf{u}_{j+1}^f}{8} G_u(\mathbf{x}_j, \mathbf{u}_j) \\ &\quad + \frac{\delta_j \mathbf{u}_{j+1}^f}{4} H_{xu}(\mathbf{x}_j, \mathbf{u}_j) + \frac{(\mathbf{u}_{j+1}^f)^2}{8} H_{uu}(\mathbf{x}_j, \mathbf{u}_j) + \frac{\delta_j^2}{8} G_x(\mathbf{x}_j, \mathbf{u}_j), \end{aligned} \quad (221)$$

and  $\mathbf{u}_{j+1}^f$  given by the first term in (216). We hence get explicit formulae for  $\bar{G}$  and  $\bar{H}$  given  $G$  and  $H$ . As for linear equations, the homogenization can be repeated. In certain cases, the form of  $G$  and  $H$  will be preserved by  $\bar{G}$  and  $\bar{H}$ , such as when

$$\begin{aligned} G(x, u) &= g_0(x, u) + \delta_j^2 g_1(x, u), \\ H(x, u) &= h_0(x, u) + \delta_j^2 h_1(x, u), \end{aligned} \quad (222)$$

where  $g_j$  and  $h_j$  are  $\mathcal{O}(1)$ .

Another approach is based on solving the nonlinear cellproblem (216) numerically, instead of using Taylor expansion, see [7]. When there is an apriori bound on  $\mathbf{u}_j$  one can discretize also in this variable. The functions  $\bar{G}$  and  $\bar{H}$  are then represented and computed on a finite grid in both arguments. This is a more expensive method, but also more accurate when  $\mathbf{u}_{j+1}^f$  is not small.

## References

1. J. Anderson. *Computational Fluid Dynamics, The Basics with Applications*. McGraw-Hill, 1995.
2. U. Andersson, B. Engquist, G. Ledfelt, and O. Runborg. A contribution to wavelet-based subgrid modeling. *Appl. Comput. Harmon. Anal.*, 7:151–164, 1999.
3. O. Axelsson. *Iterative Solution Methods*. Cambridge University Press, 1994.
4. T. M. Benson, R. J. Bozeat, and P. C. Kendall. Rigorous effective index method for semiconductor Rib waveguides. *IEE Proc. J*, 139(1):67–70, 1992.
5. A. Bensoussan, J.-L. Lions, and G. Papanicolau. *Asymptotic Analysis for Periodic Structures*. North-Holland Publ. Comp., The Netherlands, 1978.
6. G. Beylkin and M. Brewster. A multiresolution strategy for numerical homogenization. *Appl. Comput. Harmon. Anal.*, 2:327–349, 1995.
7. G. Beylkin, M. E. Brewster, and A. C. Gilbert. A multiresolution strategy for numerical homogenization of nonlinear ODEs. *Appl. Comput. Harmon. Anal.*, 5:450–486, 1998.
8. G. Beylkin, R. Coifman, and V. Rokhlin. Fast wavelet transforms and numerical algorithms I. *Comm. Pure Appl. Math.*, 44:141–183, 1991.
9. G. Beylkin and N. Coult. A multiresolution strategy for reduction of elliptic PDEs and eigenvalue problems. *Appl. Comput. Harmon. Anal.*, 5:129–155, 1998.

10. G. Beylkin, J. Dunn, and D. L. Gines. LU factorization of non-standard forms and direct multiresolution solvers. *Appl. Comput. Harmon. Anal.*, 5:156–201, 1998.
11. T. Chan and T. Mathew. The interface probing technique in domain decomposition. *SIAM J. Matrix Anal. Appl.*, 13(1):212–238, January 1992.
12. C. Concus, G. H. Golub, and G. Meurant. Block preconditioning for the conjugate gradient method. *SIAM J. Sci. Stat. Comp.*, 6:220–252, 1985.
13. I. Daubechies. *Ten Lectures on Wavelets*. SIAM, 1991.
14. M. Dorobantu and B. Engquist. Wavelet-based numerical homogenization. *SIAM J. Numer. Anal.*, 35(2):540–559, April 1998.
15. L. Durlafsky. Numerical calculation of equivalent grid block permeability tensors for heterogeneous porous media. *Water Resour. Res.*, 27:699–708, 1991.
16. Y. R. Efendiev, T. Y. Hou, and X. H. Wu. Convergence of a nonconformal multiscale finite element method. *SIAM J. Numer. Anal.*, 37:888–910, 2000.
17. B. Engquist and T. Y. Hou. Particle method approximation of oscillatory solutions to hyperbolic differential equations. *SIAM J. Num. Analysis*, 26:289–319, 1989.
18. B. Engquist and J.-G. Liu. Numerical methods for oscillatory solutions to hyperbolic problems. *Comm. Pure Appl. Math.*, 46:1–36, 1993.
19. B. Engquist and E. Luo. New coarse grid operators for highly oscillatory coefficient elliptic problems. *J. Comput. Phys.*, 129(2):296–306, 1996.
20. B. Engquist and E. Luo. Convergence of a multigrid method for elliptic equations with highly oscillatory coefficients. *SIAM J. Numer. Anal.*, 34(6):2254–2273, 1997.
21. A. C. Gilbert. A comparison of multiresolution and classical one-dimensional homogenization schemes. *Appl. Comput. Harmon. Anal.*, 5(1):1–35, 1998.
22. W. Hackbusch. *Multigrid Methods and applications*. Springer-Verlag, 1985.
23. H. A. Haus and Y. Lai. Narrow-band optical channel-dropping filter. *J. Light-wave Technol.*, 10(1):57–61, 1992.
24. T. Y. Hou and X. H. Wu. A multiscale finite element method for elliptic problems in composite materials and porous media. *J. Comput. Phys.*, 134(1):169–189, 1997.
25. T. J. R. Hughes. Multiscale phenomena: Green’s functions, the dirichlet-to neumann formulation, subgrid, scale models, bubbles and the origins of stabilized methods. *Comput. Methods Appl. Mech. Engrg.*, 127:387–401, 1995.
26. T. J. R. Hughes, G. R. Feijóo, L. Mazzei, and J.-B. Quicy. The variational multiscale method – a paradigm for computational mechanics. *Comput. Methods Appl. Mech. Engrg.*, 166:3–24, 1998.
27. O. Runborg J. Krishnan and I.G. Kevrekidis. Application of wavelet-based reduction methods to models of transport and reaction in heterogeneous media. 2001. To appear.
28. J. Keller. Geometrical theory of diffraction. *J. Opt. Soc. Amer.*, 52, 1962.
29. S. Knapek. Matrix-dependent multigrid-homogenization for diffusion problems. *SIAM J. Sci. Stat. Comp.*, 20(2):515–533, 1999.
30. D. D. Leon. *Wavelet Operators Applied to Multigrid Methods*. PhD thesis, Department of Mathematics, UCLA, 2000.
31. M. Levy, L. Eldata, R. Scarmozzino, R. M. Osgood Jr, P. S. D. Lin, and F. Tong. Fabrication of narrow-band channel-dropping filters. *IEEE Photonic. Tech. L.*, 4(12):1378–1381, 1992.

32. Z. Li. *The Immersed Interface Method—A Numerical Approach for Partial Differential Equations with Interfaces*. PhD thesis, Department of Applied Mathematics, Univ. of Washington, 1994.
33. A.-M. Matache and C. Schwab. Homogenization via  $p$ -FEM for problems with microstructure. *Appl. Numer. Math.*, 33:43–59, 2000.
34. N. Neuss. *Homogenisierung und Mehrgitter*. PhD thesis, Fakultät Mathematik Universität Heidelberg, 1995.
35. N. Neuss, W. Jäger, and G. Wittum. Homogenization and multigrid. Preprint 98-04 (SFB 359), 1998.
36. P.-O. Persson and O. Runborg. Simulation of a waveguide filter using wavelet-based numerical homogenization. *J. Comput. Phys.*, 166:361–382, 2001.
37. V. Ramaswamy. Strip-loaded film waveguide. *Bell Syst. Tech. J.*, 53:697–705, 1974.
38. J. W. Ruge and K. Stüben. Algebraic multigrid. In *Multigrid Methods*, Frontiers in Applied Mathematics, pages 73–170. SIAM, 1987.
39. O. Runborg. *Multiscale and Multiphase Methods for Wave Propagation*. PhD thesis, Department of Numerical Analysis and Computing Science, KTH, Stockholm, 1998.
40. F. Santosa and M. Vogelius. First order corrections to the homogenized eigenvalues of a periodic composite medium. *SIAM J. Appl. Math.*, 53:1636–1668, 1993.
41. B. Z. Steinberg, J. J. McCoy, and M. Mirotznik. A multiresolution approach to homogenization and effective modal analysis of complex boundary value problems. *SIAM J. Appl. Math.*, 60(3):939–966, 2000.
42. A. Taflove. *Computational Electromagnetics, The Finite-Difference Time-Domain Method*, chapter 10. Artech House, 1995.
43. L. Tartar. *Etudes des oscillations dans les equations aux dérivées partielles non linéaires*, volume 195 of *Lecture Notes in Physics*, pages 384–412. Springer-Verlag, 1984.
44. D. Wilcox. *Turbulence Modeling for CFD*. DCW Industries, Inc., 1993.